

Addressing Positivity Violations in Continuous Interventions through Data-Adaptive Strategies

Han Bao^{*1} and Michael Schomaker^{1,2,3,4}

¹Department of Statistics, Ludwig-Maximilians-Universität München, Munich, Germany

²Centre for Integrated Data and Epidemiological Research, Cape Town, South Africa

³Institute of Public Health, Medical Decision Making and Health Technology Assessment, UMIT – University for Health Sciences, Medical Informatics and Technology, Hall in Tirol, Austria

⁴Munich Center for Machine Learning (MCML), Ludwig-Maximilians-Universität München, Munich, Germany

Abstract

Positivity violations pose a key challenge in the estimation of causal effects, particularly for continuous interventions. Current approaches for addressing this issue include the use of weights or modified treatment policies. While effective in many contexts, these methods can result in estimands that do not always align well with the original research question, thereby compromising interpretability.

In this paper, we introduce a novel diagnostic tool—the non-overlap ratio—to detect positivity violations. To address these violations while maintaining interpretability, we propose a data-adaptive solution, specifically the “most feasible” intervention strategy.

Our strategy operates on a unit-specific basis. For a given intervention of interest, we first assess whether the intervention value is feasible for each unit. For units with sufficient support—conditional on confounders—we adhere to the intervention of interest. However, for units lacking sufficient support, we do not assign the actual intervention value of interest. Instead, we assign the closest feasible value within the support region. The non-overlap ratio provides a diagnostic summary of such support across the population.

We propose an estimator using g-computation coupled with flexible conditional density estimation to identify high- and low-support regions and to estimate this new estimand. Through simulations, we demonstrate that our method effectively reduces bias across various scenarios by addressing positivity violations. Moreover, when positivity violations are absent, the method successfully recovers the standard estimand. We further validate its practical utility using real-world data from the CHAPAS-3 trial, which enrolled HIV-positive children in Zambia and Uganda.

Keywords: data-adaptive interventions; causal inference; positivity violations; HIV treatment

1 Introduction

Causal inference methods have been extensively studied for binary treatments, where individuals are either exposed to a treatment or assigned to a control condition [21, 17]. In this framework, the positivity assumption—requiring that each individual has a non-zero probability of receiving any treatment level under consideration within confounder strata—is crucial for the identifiability and unbiased estimation of causal effects.

Violations of the positivity assumption can be categorized as structural or practical [38, 27, 37]. Structural violations occur when an intervention is inherently impossible, whereas practical violations arise when certain treatment levels are theoretically possible but are not observed in the data. Both types lead to non-overlap in the confounder space, where certain confounder patterns have a zero probability—either theoretical or

^{*}Corresponding author. Email: han.bao@stat.uni-muenchen.de

estimated—of receiving specific treatment levels. These violations hinder the estimation of causal effects, making it challenging to draw reliable inferences.

In pharmacoepidemiological and public health studies, researchers often extend their focus to continuous interventions, where the treatment variable can take on a range of values. In this context, the estimation of the causal dose-response curve (CDRC)—which describes the relationship between the continuous treatment and the outcome—has gained increasing attention in the causal inference literature. The CDRC provides a nuanced understanding of the causal effects of continuous interventions. However, estimating the CDRC introduces new challenges, particularly because the identification of the CDRC necessitates a more restrictive positivity assumption, requiring that the conditional treatment density is greater than zero—which, when interpreted strictly, is never fully met.

For continuous interventions, the positivity assumption is commonly violated due to the infinite dimensionality of the treatment space. This makes it virtually impossible to observe all potential treatment levels across all confounder combinations. The resulting sparsity in certain regions of the intervention space can lead to unstable or biased estimates—a challenge frequently overlooked in existing studies.

While methods adapted from binary treatments can be applied, they have limitations. Trimming, for example, excludes regions of the confounder space with poor overlap [7], removing individuals with extreme probabilities of treatment given their confounders. However, this approach may result in the loss of valuable data.

To tackle these challenges, researchers have developed specialized methods, including projection functions and g-computation-type plug-in estimators, which aim to mitigate the violation of the positivity assumption [27]. One such approach is the weighted CDRC, which reweights and redefines the estimand of interest based on functions of the conditional support for the respective interventions [31]. Additionally, machine learning techniques have proven effective in enhancing estimation accuracy by minimizing the risk of bias caused by model misspecification [25].

Another notable strategy involves modified treatment policies (MTPs)[11, 9], which specify systematic modifications to the observed (natural) treatment, with the goal of avoiding interventions among individuals for whom the treatment would be infeasible. When designed carefully, MTPs can substantially reduce reliance on the positivity assumption. However, they typically target a different causal estimand than the causal dose-response curve (CDRC), which may or may not align with the scientific objectives of a particular study—including the empirical example discussed in Section 5. MTPs are most useful when the modified intervention itself is of substantive scientific interest. Haneuse and Rotnitzky provide an example of a very well-motivated MTP [11].

While double robustness and semiparametric efficiency are desirable properties, they are not always achievable when estimating the full CDRC under continuous interventions. In fact, under only mild smoothness conditions, the CDRC is not pathwise differentiable [8], precluding the construction of root- n consistent or doubly robust estimators without additional structure. Recent work has developed doubly robust estimators under assumptions such as differentiability [22], monotonicity [36], or smooth invertibility [9], but these assumptions may not be justified in many applied settings—especially when the estimand is defined by the scientific question and not chosen for statistical convenience.

In this paper, we pursue a complementary goal: to preserve the original CDRC as the target estimand while improving its identifiability and estimation by redefining the intervention space in a data-adaptive way. This leads to a natural plug-in strategy that avoids extrapolation into unsupported regions, thereby enhancing both interpretability and applicability in the presence of positivity violations. Although such estimators are not doubly robust, they remain closely aligned with the scientific question, offer clear interpretability, and reduce sensitivity to model misspecification by focusing estimation in well-supported regions. Our specific contributions are:

1. Defining and diagnosing positivity violations in practice: we introduce a framework for assessing positivity in continuous interventions. Specifically, we define the support using the highest density region of the conditional intervention distribution and propose the non-overlap ratio—a population-level diagnostic that summarizes the extent of non-overlap across confounder strata, thereby quantifying the severity of positivity violations.
2. Introducing novel estimands to address positivity violations: we propose a framework of data-adaptive interventions—specifically, the most feasible intervention—to construct a new estimand that replaces

infeasible interventions with the closest feasible values based on the observed data. This approach improves both interpretability and applicability, allowing researchers to approximate the standard CDRC without significantly deviating from the original intervention strategy.

By addressing the challenges posed by positivity violations in continuous interventions, our proposed methods provide a practical and reliable framework for causal inference. We demonstrate the effectiveness of our approach through simulations and real data analysis, highlighting the advantages of our method in mitigating positivity violations while preserving interpretability through minimal adjustments to the infeasible interventions.

2 From Identification Assumptions to Positivity Violations

2.1 Notation

We consider the following setup:

- Y : outcome, taking values in \mathcal{Y} .
- A : treatment (or exposure), taking values in \mathcal{A} .
- $\mathbf{L} = (L_1, \dots, L_q)$: vector of $q \in \mathbb{N}$ confounders, taking values in \mathcal{L} .
- Temporal ordering: $L_1, \dots, L_q \rightarrow A \rightarrow Y$.

Uppercase letters denote random variables, and lowercase letters their realizations. We adopt the potential outcome framework [29]: for subject i , Y_i^a denotes the counterfactual outcome that would be observed if A_i were set to level $a \in \mathcal{A}$.

Let $O = (\mathbf{L}, A, Y)$ denote a generic observation, with true distribution P_0 . The observed data are

$$O_1, \dots, O_n \stackrel{\text{iid}}{\sim} P_0.$$

We use the following notation for distributions and densities:

- The marginal distribution of A is P_A , with density f_A .
- The marginal distribution of \mathbf{L} is $P_{\mathbf{L}}$, with density $f_{\mathbf{L}}$.
- The conditional distribution of A given \mathbf{L} is $P_{A|\mathbf{L}}$, with density $f_{A|\mathbf{L}}$.

Throughout, P_0 denotes the true distribution, P a generic distribution (in theoretical results), and P_n the empirical distribution.

2.2 Determination of Positivity Violations

In causal inference, assumptions such as consistency, exchangeability, and positivity are critical for identifying causal effects. Among these, positivity—often regarded as straightforward—plays a unique role in ensuring that causal treatment effects can be properly identified.

Formally, the positivity assumption requires that every treatment level has positive probability within each stratum of the confounders \mathbf{L} [27]:

$$\inf_{a \in \mathcal{A}} f_{A|\mathbf{L}}(a \mid \mathbf{L}) > 0, \quad \text{a.e.} \quad (1)$$

That is, the conditional treatment density must be bounded away from zero across the entire intervention space \mathcal{A} , with the precise requirement depending on the distribution of the intervention. While positivity is typically discussed as an abstract identification assumption, less attention has been paid to detecting violations in practice.

Even when identification holds, sparse data in certain regions of the intervention space can severely affect bias and precision at the estimation stage (see Appendix A for details). Reliable causal estimation

becomes difficult when parts of the intervention domain are poorly represented for some confounder patterns, introducing bias and limiting the generalizability of the estimated causal effects.

Determining whether the data provide sufficient support for a given intervention requires assessing whether the density is so low that observing it in finite samples becomes nearly impossible. This motivates introducing a threshold c on the density function to identify potential positivity violations, as proposed by Schomaker et al. [31]. Given a specific realization of confounders, $\mathbf{L} = \mathbf{l}$, an intervention of interest a can be classified as:

$$\begin{cases} \text{supported,} & \text{if } f_{A|\mathbf{L}}(a | \mathbf{l}) > c, \\ \text{not supported,} & \text{if } f_{A|\mathbf{L}}(a | \mathbf{l}) \leq c. \end{cases} \quad (2)$$

For binary interventions, (near-)violations occur when the conditional probability of observing an intervention is extremely small or zero. In this discrete case, densities coincide with probabilities, making violations relatively straightforward to detect. For continuous interventions, however, the situation is more complex. The density function must satisfy

$$\int_{\mathcal{A}} f(a) da = 1,$$

so the scale of f depends on the size of the intervention space \mathcal{A} . This variability complicates the use of static thresholds; for instance, defining interventions as unsupported when $f < 0.001$ or as sufficiently supported when $f > 0.1$ may not be meaningful across different contexts.

Because of this, fixed thresholds are problematic for continuous interventions. To address this limitation, we propose a novel dynamic diagnostic measure that redefines and more accurately determines positivity violations in practical settings.

2.3 Proposal 1: Definition of Support and Diagnostic Using Highest Density Regions (HDRs)

2.3.1 Conditional support via highest density regions

To address the issue of poorly supported intervention areas, we propose a method that dichotomizes the normalized density values. This approach identifies regions of the intervention space \mathcal{A} where support is either adequate or lacking, based on a probability threshold. Specifically, we partition \mathcal{A} into two sets, $\mathcal{A}_\alpha(\mathbf{l})$ and its complement $\mathcal{A}_\alpha^c(\mathbf{l})$, according to a specified threshold depending on \mathbf{l} . Given a threshold for non-overlap detection, referred to as the **support level** α , the set $\mathcal{A}_\alpha(\mathbf{l})$ is defined such that

$$P(\mathcal{A}_\alpha(\mathbf{l})) = \alpha.$$

An intervention a can then be categorized as

$$\begin{cases} \text{supported,} & \text{if } a \in \mathcal{A}_\alpha(\mathbf{l}), \\ \text{not supported,} & \text{if } a \notin \mathcal{A}_\alpha(\mathbf{l}). \end{cases} \quad (3)$$

We define $\mathcal{A}_\alpha(\mathbf{l})$ using highest density regions (HDRs), which represent the practical support of the intervention. This concept, introduced by Hyndman [20], is formally given by

$$\mathcal{A}_\alpha(\mathbf{l}) = \{a \in \mathcal{A} : f_{A|\mathbf{L}}(a | \mathbf{l}) \geq f_\alpha\}, \quad (4)$$

where f_α is a threshold chosen such that

$$P_{A|\mathbf{L}=\mathbf{l}}(\mathcal{A}_\alpha(\mathbf{l})) = \alpha.$$

Figure 1 illustrates this idea: the green regions indicate the conditional support where interventions are well-supported by the data, while the grey regions highlight areas of positivity violations. In this example, the total probability of the green region corresponds to a **support level** of $\alpha = 0.95$.

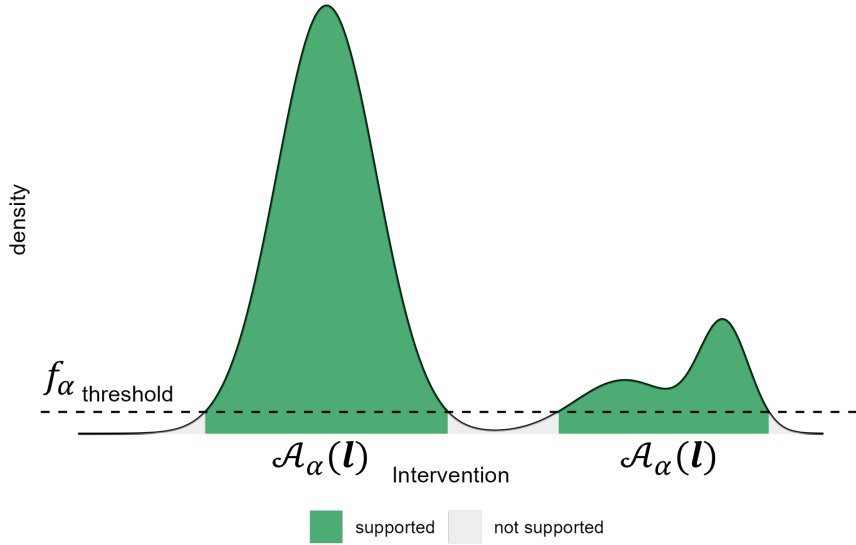


Figure 1: Illustration of using highest density regions as conditional support. Green areas indicate well-supported interventions, while grey areas correspond to positivity violations.

2.3.2 Diagnostic measure: the non-overlap ratio

To assess positivity in practice, we introduce the **non-overlap ratio**. This diagnostic summarizes, at the population level, the extent to which a candidate intervention value a falls outside the conditional support region defined by the HDRs. Formally, we define a function $\tau : \mathcal{A} \rightarrow [0, 1]$ by

$$\tau(a) := \int \mathbb{1}\{a \notin \mathcal{A}_\alpha(\mathbf{L})\} dP_{\mathbf{L}}. \quad (5)$$

Here, $\tau(a)$ represents the proportion of individuals whose covariate profiles \mathbf{L} render the intervention value a unsupported, i.e., lying outside the practical support region where the positivity assumption is satisfied.

The non-overlap ratio takes values between 0 and 1:

- Values near 0 indicate that a is well-supported across the population, with few or no positivity violations at the chosen support level.
- Values near 1 indicate that a is largely unsupported, reflecting severe positivity violations and suggesting that causal inferences at this value are unreliable.

By aggregating individual-level support into a single summary, the non-overlap ratio provides a population-level diagnostic for evaluating the plausibility of the positivity assumption. Its practical use will be illustrated in the following sections.

3 Estimands to Address Positivity Violations

3.1 Standard Causal Dose–Response Curve

Estimand 1 (Standard)

The standard causal dose–response curve is the function $m^{\text{standard}} : \mathcal{A} \rightarrow \mathcal{Y}$ defined by

$$m^{\text{standard}}(a) = \mathbb{E}(Y^a),$$

which can be identified as

$$\begin{aligned}
m^{\text{standard}}(a) &\stackrel{(i)}{=} \mathbb{E}[\mathbb{E}(Y^a \mid A = a, \mathbf{L})] \\
&\stackrel{(ii)}{=} \mathbb{E}[\mathbb{E}(Y \mid A = a, \mathbf{L})] \\
&= \int \mathbb{E}(Y \mid A = a, \mathbf{L} = \mathbf{l}) dP_{\mathbf{L}}(\mathbf{l}),
\end{aligned} \tag{6}$$

where equality (i) follows by the law of iterated expectations and conditional exchangeability, and equality (ii) by consistency and the positivity assumption (Equation 1).

The standard causal dose-response curve, reliant on the positivity assumption in Equation 1, faces serious challenges due to frequent violations, particularly with continuous interventions. As the intervention range widens, regions of the confounder space often have limited or no support, so that $\hat{f}(a \mid \mathbf{L})$ approaches zero. In such cases, identification fails and estimation becomes unstable.

This difficulty is magnified in practice because continuous exposures span infinitely many potential values, making it impossible to observe all treatment levels across every confounder pattern in finite samples. Consequently, estimation procedures are forced to extrapolate into sparsely or never observed regions of the intervention space. Such extrapolation produces unstable estimates, inflates standard errors, and introduces bias, thereby compromising both the validity and the generalizability of the estimated dose-response relationship.

3.2 Existing Estimand to Address Positivity Violations: Weighted Causal Dose-Response Curve

Estimand 2 (Weighted CDRC)

Schomaker et al. [31] propose the weighted CDRC, defined as

$$\begin{aligned}
m^{\text{weighted}}(a) &:= \mathbb{E}(Y^a \mid f(a \mid \mathbf{L}) > c) P(f(a \mid \mathbf{L}) > c) \\
&\quad + \mathbb{E}(Y^a w(a \mid \mathbf{L}) \mid f(a \mid \mathbf{L}) \leq c) P(f(a \mid \mathbf{L}) \leq c), \quad \forall a \in \mathcal{A},
\end{aligned} \tag{7}$$

which admits the identification formula

$$m^{\text{weighted}}(a) = \int \mathbb{E}(Y \mid A = a, \mathbf{L} = \mathbf{l}) w(a, \mathbf{l}) dP_{\mathbf{L}}(\mathbf{l}), \tag{8}$$

where the weight function $w(a, \mathbf{l})$ is given by

$$w(a, \mathbf{l}) = \begin{cases} 1, & \text{if } f(a \mid \mathbf{l}) > c, \\ \frac{f(a \mid \mathbf{l})}{f(a)}, & \text{if } f(a \mid \mathbf{l}) \leq c. \end{cases} \tag{9}$$

The weighted CDRC mitigates positivity violations by coinciding with the standard estimand in regions with adequate support, and by redefining it in regions with limited support through a projection based on conditional densities. This ensures identifiability and avoids extrapolation into unsupported regions. However, it changes the target parameter: the resulting curve no longer represents the causal effect of assigning all individuals to treatment level a , but rather a blend of causal and weighted associational components. As a consequence, the weighted CDRC may diverge from the scientific estimand of interest, and its causal interpretation becomes less transparent.

More broadly, this approach highlights a fundamental trade-off in addressing positivity violations: one can either preserve the original scientific estimand but accept estimation that is potentially unstable, highly variable, or biased in regions with sparse data, or redefine the estimand to guarantee identifiability at the cost of causal interpretability. The weighted CDRC takes the latter path, producing well-defined estimates that avoid extrapolation into unsupported regions, but in doing so it targets a modified scientific question.

In applied settings, researchers must therefore balance the benefits of improved precision and robustness against the loss of a direct causal interpretation when deciding whether to adopt the weighted CDRC.

3.3 Novel Estimands to Address Positivity Violations: Causal Dose–Response Curve with Data-Adaptive Intervention

To address these challenges, we propose a novel estimand that mitigates the impact of positivity violations by focusing on well-supported regions of the intervention space, guided by the diagnostic tool proposed in the previous section. This approach relaxes the strict positivity requirement by focusing on empirically supported regions of the intervention space, while maintaining interpretability of the resulting causal estimand.

3.3.1 Data-Adaptive Intervention

Unlike static interventions, which assign a fixed treatment a to all units, we introduce a more refined approach called the *data-adaptive intervention*. This strategy customizes the intervention for each individual based on their confounders and the observed data.

For a given oracle intervention value a , the idea can be summarized schematically as

$$\begin{cases} \text{intervene with } a, & \text{if } a \text{ is supported in the data,} \\ \text{intervene adaptively,} & \text{otherwise.} \end{cases} \quad (10)$$

Formally, let $\mathcal{A}_\alpha(\mathbf{l}; P)$ denote the highest density regions (HDRs) of treatment values supported by the distribution P given covariates \mathbf{l} , as defined in Section 2.2.

We define the *data-adaptive intervention operator*

$$d : \mathcal{A} \times \mathcal{L} \times \mathcal{P} \rightarrow \mathcal{A},$$

where \mathcal{P} denotes the space of candidate distributions. The operator assigns to each (a, \mathbf{l}, P) a feasible treatment value via

$$d(a, \mathbf{l}; P) = \begin{cases} a, & \text{if } a \in \mathcal{A}_\alpha(\mathbf{l}; P), \\ h(a, \mathbf{l}; P), & \text{otherwise,} \end{cases} \quad (11)$$

where $h : \mathcal{A} \times \mathcal{L} \times \mathcal{P} \rightarrow \mathcal{A}$ is a *substitution function* satisfying

$$h(a, \mathbf{l}; P) \in \mathcal{A}_\alpha(\mathbf{l}; P) \quad \text{whenever } a \notin \mathcal{A}_\alpha(\mathbf{l}; P). \quad (12)$$

The corresponding counterfactual outcome under the data-adaptive intervention is denoted

$$Y^d \equiv Y^{d(a, \mathbf{l}; P)}.$$

In practice, the true distribution P is unknown and replaced by the empirical distribution P_n , which makes the rule inherently *data-adaptive*. For notational convenience, write

$$\mathcal{A}_\alpha(\mathbf{l}) := \mathcal{A}_\alpha(\mathbf{l}; P_n) \quad \text{and} \quad h(a, \mathbf{l}) := h(a, \mathbf{l}; P_n).$$

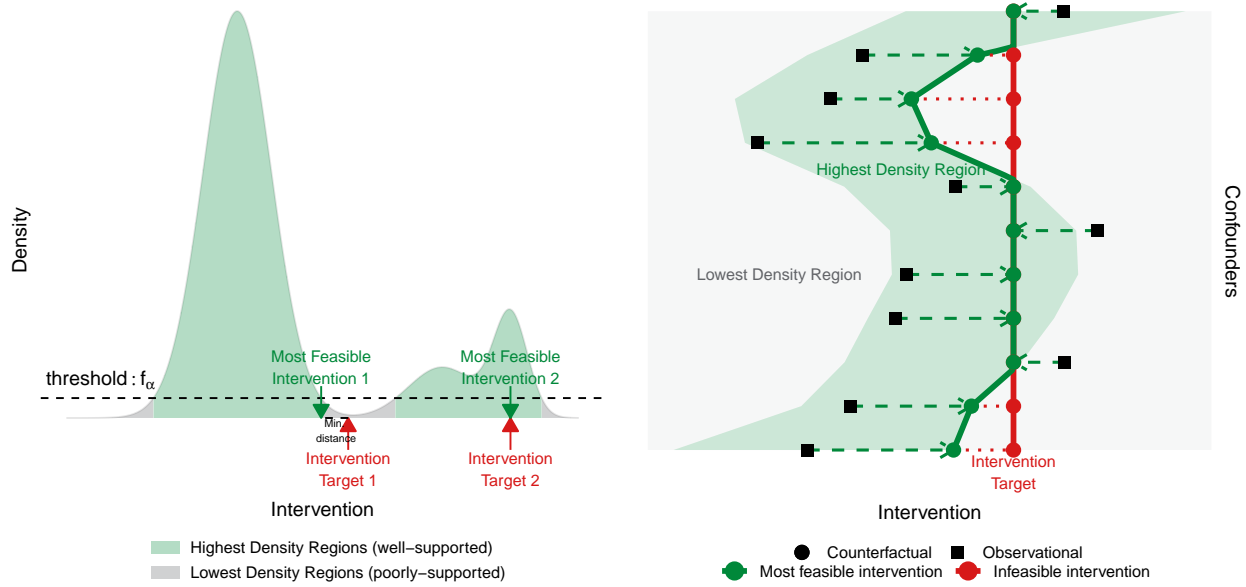
Then the data-adaptive intervention rule becomes

$$d(a, \mathbf{l}; P_n) = \begin{cases} a, & \text{if } a \in \mathcal{A}_\alpha(\mathbf{l}), \\ h(a, \mathbf{l}), & \text{otherwise.} \end{cases} \quad (13)$$

3.3.2 The Most Feasible Intervention

A natural choice for the substitution function h is to reassign unsupported interventions to the nearest feasible value, ensuring minimal deviation from the intended intervention:

$$h(a, \mathbf{l}) = \arg \min_{a^* \in \mathcal{A}_\alpha(\mathbf{l})} |a^* - a|. \quad (14)$$



(a) Targets outside the HDRs are reassigned to the closest feasible value within the HDRs. The green shaded area represents the highest density region (well-supported interventions), the grey area indicates regions with little or no support, and the dashed line marks the density threshold f_α . Red arrows denote target interventions: Target 1 lies outside the HDR and is reassigned to the nearest feasible value (Most Feasible Intervention 1), while Target 2 lies within the HDR and is retained unchanged (Most Feasible Intervention 2).

(b) Targets inside the HDRs remain unchanged, while unsupported targets are shifted adaptively. Red circles denote target interventions, green circles represent their most feasible reassigned values, and black squares indicate observed data points across strata of the confounders. Green shaded areas indicate HDRs, while grey areas mark unsupported regions. This illustrates how infeasible interventions are reassigned adaptively to the closest feasible value, ensuring that interventions are only minimally adjusted.

Figure 2: Illustration of the most feasible intervention defined in Equations 13 and 14. Panel (a) shows the conditional density of treatment values given covariates, with HDRs (green) representing well-supported regions and grey areas denoting poorly supported regions. Target interventions (red arrows) are either retained if they fall inside HDRs or reassigned to the nearest feasible value within HDRs (green arrows). Panel (b) extends this principle across confounder strata, where targets (red circles) are reassigned to the closest supported value (green circles) whenever they fall outside HDRs, while feasible targets remain unchanged. Together, the panels illustrate the principle of the most feasible intervention: retain the target when supported, and otherwise make the smallest necessary adjustment to ensure feasibility.

An illustration is provided in Figure 2a. The horizontal axis shows intervention values and the vertical axis their estimated conditional density. Green shaded areas mark the highest density regions (HDRs), where the conditional density exceeds the threshold f_α (dashed line) and interventions are well supported; grey areas indicate poorly supported regions. The red arrows denote hypothetical targets: Target 1 lies outside the HDR, while Target 2 lies inside. Under the proposed rule, unsupported targets are reassigned to the nearest feasible value within the HDRs (green arrows). Thus, Target 1 shifts to the closest HDR point, while Target 2 remains unchanged. This illustrates the principle of the most feasible intervention: retain the target if supported, otherwise reassign it to the nearest supported value.

3.3.3 Proposal 2: A Novel Estimand Based on Feasible Interventions

Estimand 3 (Feasible)

With the definitions of support and the substitution function in Equations 4 and 14, the proposed

estimand is

$$m^{\text{feasible}}(a) = \mathbb{E}(Y^d), \quad (15)$$

where d is defined in Equation 13 and h in Equation 14. Equivalently,

$$m^{\text{feasible}}(a) = \mathbb{E}\left[Y^a \mathbb{1}\{a \in \mathcal{A}_\alpha(\mathbf{L})\} + Y^{h(a, \mathbf{L})} \mathbb{1}\{a \notin \mathcal{A}_\alpha(\mathbf{L})\}\right]. \quad (16)$$

In words, each unit either (i) receives the target intervention a if a lies in its supported region $\mathcal{A}_\alpha(\mathbf{L})$, or (ii) is reassigned to the nearest feasible value $h(a, \mathbf{L})$ otherwise. The resulting curve averages these counterfactuals across the population, yielding a causal dose-response curve that closely aligns with the original estimand while remaining identifiable in the presence of positivity violations. By limiting substitutions to the minimal adjustment necessary, this approach preserves interpretability and avoids the distortions introduced by extrapolation into unsupported regions.

Comparison of Estimand 2 and Estimand 3 Both the weighted CDRC and the feasible CDRC aim to address positivity violations by restricting attention to regions with sufficient empirical support. However, they adapt the estimand in fundamentally different ways. The weighted CDRC of Schomaker et al. [31] applies a fixed cutoff c to the conditional density and redefines the target through projection weights. This ensures identifiability without requiring extrapolation, but it alters the causal parameter: in regions of support, the curve coincides with the standard CDRC, while in unsupported strata it relies on weighted associational components. As Schomaker et al. emphasize, this means the weighted curve sticks to the causal question where feasible but falls back on associations where necessary, yielding a compromise between interpretability and stability. By contrast, the feasible CDRC employs a unit-specific, data-adaptive threshold and modifies intervention assignments explicitly by reassigning unsupported values to the closest feasible ones. This produces a transparent intervention rule targeting the well-defined quantity $E(Y^d)$. In short, the weighted CDRC trades some causal interpretability for broader identifiability, whereas the feasible CDRC preserves interpretability while adapting directly to the observed support.

Interpretation Figure 2b illustrates how the most feasible intervention strategy operates at the individual level, conditional on confounders. The vertical axis represents confounder values, and the horizontal axis represents the intervention. The shaded green band marks the highest density regions, where intervention values are well supported by the data, while the surrounding grey area corresponds to lowest density regions with little or no support. The red vertical line indicates the oracle intervention target, which may not be feasible for all individuals. Units whose oracle intervention lies outside the highest density regions (shown as red circles) cannot be assigned this target directly. Instead, the proposed rule reassigns them to the nearest feasible value within the highest density regions, shown by the green circles and arrows. By contrast, units whose oracle target already falls within the highest density regions (green circles on the red line) retain their original assignment. Black squares represent the observed data (intervention-confounder pairs), from which the highest density regions are estimated. Overall, the figure demonstrates that the most feasible intervention rule systematically reassigns unsupported targets to the closest feasible values, ensuring that every individual receives an intervention assignment compatible with the observed data distribution.

Violations of the positivity assumption are not merely theoretical concerns but also reflect real-world scenarios where certain interventions are impractical or unrealistic for specific subpopulations. For example, consider drug concentration levels across patients, as discussed in Section 5. Patients with a fast metabolism, who metabolize drugs rapidly, naturally exhibit low drug concentrations even when administered standard doses. For these patients, a high drug concentration target would be unrealistic because it would require doses far beyond what is commonly observed or safely prescribed. While theoretically possible, achieving such concentrations would involve dosing regimens that are rarely practiced due to clinical and practical concerns. This leads to a situation where data corresponding to such high concentrations is either extremely sparse or non-existent, resulting in biased causal inferences and making conclusions drawn from such targets unreliable.

The proposed CDRC with the **most feasible intervention** addresses these issues by adapting the intervention target to stay within regions where data are sufficiently abundant and well-supported. Instead of forcing an unrealistic target that fails to align with real-world conditions, this approach adjusts the

intervention based on what is practically achievable and observable within the data. This has two key benefits: first, it reduces bias caused by data sparsity and positivity violations, and second, it ensures that the causal effects being estimated are relevant and actionable in practice.

Unlike fixed interventions, which risk oversimplifying causal relationships by imposing uniform targets, the most feasible intervention approach offers a more nuanced and reasonable strategy. It acknowledges the inherent variability in real-world data and adapts the intervention accordingly, leading to more robust, reliable, and meaningful causal inferences that better reflect both the data and the practical realities of clinical and observational settings.

3.3.4 Data-Adaptive Trimming Causal Dose–Response Curve

In causal estimation, *trimming* refers to the practice of excluding observations with insufficient treatment support in order to stabilize estimation and mitigate the impact of positivity violations [7]. In its classical form, trimming relies on a fixed threshold $c > 0$ applied to the conditional treatment density, yielding

$$m^{\text{trimming}}(a) : a \mapsto \mathbb{E}(Y^a \mid f_{A|\mathbf{L}}(a \mid \mathbf{L}) > c), \quad (17)$$

where $f_{A|\mathbf{L}}$ is the conditional density of A given \mathbf{L} .

Estimand 4 (Trimming)

In our framework, trimming is expressed in a more flexible, *data-adaptive* way using the empirical feasible set $\mathcal{A}_\alpha(\mathbf{L})$ introduced in Section 2.2. Specifically, we define

$$m^{\text{trimming}}(a) : a \mapsto \mathbb{E}(Y^a \mid a \in \mathcal{A}_\alpha(\mathbf{L})), \quad (18)$$

that is, the mean counterfactual outcome restricted to those units for whom the intervention value a lies within the empirically supported region given their covariates.

This estimand can be identified by

$$\int \mathbb{E}(Y \mid A = a, \mathbf{L}) t(a, \mathbf{L}) dP_{\mathbf{L}}(\mathbf{l}), \quad (19)$$

where the trimming weight is

$$t(a, \mathbf{l}) = \begin{cases} \frac{1}{\tau}, & \text{if } a \in \mathcal{A}_\alpha(\mathbf{L}), \\ 0, & \text{otherwise,} \end{cases} \quad (20)$$

with $\tau = P_0(a \in \mathcal{A}_\alpha(\mathbf{L}))$ denoting the probability that a falls within the empirical feasible region.

Comparison: This data-adaptive trimming estimand improves upon classical trimming by replacing an arbitrary, fixed threshold with a threshold derived from the observed distribution of the data. In doing so, it ensures that only well-supported units contribute to estimation, while retaining interpretability by conditioning on the feasible region. However, like classical trimming, it targets a restricted population rather than the full sample, which may reduce generalizability. In contrast, the feasible CDRC (Estimand 3) reassigns unsupported interventions rather than excluding them, preserving the entire study population while still avoiding extrapolation.

3.4 Estimation

3.4.1 Causal Estimation

To estimate the standard CDRC in Equation (6), a parametric g-formula can be readily applied for single time-point interventions. Substitution (plug-in) estimators can also be constructed to estimate the data-adaptive estimands introduced in Equation (15) and (18), with the full procedure detailed in Algorithm 1.

Notes:

- 1) The estimated conditional treatment density $\hat{f}(a | \mathbf{l})$ (Step 2) is used only to define the data-adaptive estimands (feasible and trimming) and does not enter into the estimation of the outcome model.
- 2) Valid statistical inference using bootstrap intervals (Step 6) requires, under standard regularity, estimators that are \sqrt{n} -consistent and asymptotically linear with a well-defined influence function[3, 34, 35, 23]. These conditions are satisfied, for example, by correctly specified parametric outcome models, and can also be met by certain flexible estimators such as the Highly Adaptive Lasso (HAL) [2], which under mild conditions yields plug-in estimators that are \sqrt{n} -consistent and asymptotically linear in pathwise differentiable settings [6, 33]. The CDRC, however, is not pathwise differentiable as a full curve, so bootstrap validity cannot be guaranteed in general. At best, bootstrap may provide pointwise inference at fixed treatment values under correct parametric specification. In contrast, HAL plug-in estimators of the CDRC are pointwise asymptotically normal under undersmoothing, which enables valid delta-method inference based on the influence curve of the HAL coefficients [32]. This approach is analogous to the empirical sandwich variance estimator recently proposed for ICE g-computation by Zivich et al. [39].
- 3) When the target estimand is defined in a data-adaptive manner—such as via estimated highest density regions—standard independence assumptions are violated. As emphasized by Hubbard et al.[19], the intervention assigned to a given unit depends on functions of the data estimated from other units, introducing dependence between the observed data and the target parameter. This dependence may affect the validity of standard inferential procedures such as the bootstrap.
- 4) A proposed remedy is sample splitting or cross-validation, whereby the data-adaptive rule is defined on one subset of the data and the parameter is estimated on another. This restores approximate independence between the estimand and the estimation process. However, such approaches introduce practical complexity: they yield multiple, split-specific estimands, and averaging across them may reduce interpretability.
- 5) In this work, we choose to use the full sample to define and estimate the data-adaptive estimands. This preserves a single, coherent target parameter that reflects the region of intervention support within the observed data. While this choice introduces some additional dependence between the data and the estimand, we view it as a pragmatic balance between interpretability and statistical rigor.
- 6) Our simulation study (Appendix D) includes an empirical evaluation of bootstrap coverage, both with and without sample splitting. In the settings considered, bootstrap intervals achieve coverage close to nominal levels in well-supported regions. Thus, the practical benefit in interpretability outweighs the modest loss of conservativeness in inference for many applied scenarios.

3.4.2 Conditional Density Estimation

A key step in this process involves estimating the conditional density of the intervention given the confounders. Accurate conditional density estimation is essential for characterizing the regions in which the oracle intervention is supported by the data. Several approaches can be employed, including parametric models, nonparametric kernel conditional density estimators [12], and more flexible methods such as the Highly Adaptive Lasso-based density estimator (Haldensify) [13, 16, 14]. Motivated by Haldensify, in this paper we adopt a hazard-binning-based conditional density estimator, described in Appendix C, which is closely related to the approach of Díaz et al.[10]. This class of estimators can flexibly approximate conditional densities even when the relationship between confounders and interventions is complex or highly nonlinear.

4 Simulation Studies

In this section, we examine the proposed methods through three distinct simulation settings. These simulations are designed to provide insight into the performance of the methods under different conditions.

In Simulation 1, we explore how positivity violations exacerbate bias in causal estimates, particularly when the outcome models are misspecified. Simulation 2 examines the impact of positivity violations on causal estimation by comparing scenarios with and without positivity violations. Simulation 3 investigates

Algorithm 1 Estimation Algorithm for m^{standard} , m^{feasible} , m^{trimming} , and τ

1: Set-Up:

- Let n denote the number of subjects.
- Define a grid of m intervention values: $\bar{\mathbf{a}} = (a_1, \dots, a_m)^T$.
- Choose a support level α to define highest density regions (HDRs).

2: Estimate Highest Density Regions:

- (a) **Conditional Density Estimation:** Estimate the conditional treatment density $\hat{f}(a | \mathbf{l})$ using the observed data, and evaluate $\hat{f}(a_i | \mathbf{l}_j)$ for all $i = 1, \dots, m$ and $j = 1, \dots, n$.
- (b) **Density Thresholds:** For each subject j , determine \hat{f}_α^j , the threshold such that the estimated HDR for subject j contains probability mass α .

3: Compute the Non-Overlap Ratio:

$$\hat{\tau}(a_i) = \frac{1}{n} \sum_{j=1}^n I(\hat{f}(a_i | \mathbf{l}_j) < \hat{f}_\alpha^j)$$

4: Estimate the Outcome Model:

- Estimate the conditional outcome model $\hat{E}(Y | A, \mathbf{L})$, for example using parametric regression.
- *Note:* For plug-in estimation and bootstrap inference, we recommend outcome models with established theoretical guarantees (e.g., parametric models). Flexible methods such as HAL can also be considered.

5: Causal Estimation via Plug-in Estimators:

(b) **Standard Estimand:**

$$\hat{m}^{\text{standard}}(a_i) = \frac{1}{n} \sum_{j=1}^n \hat{E}(Y | A = a_i, \mathbf{l}_j)$$

(b) **Feasible Estimand:**

- For each a_i and subject j : if $\hat{f}(a_i | \mathbf{l}_j) < \hat{f}_\alpha^j$, set $\hat{d}(a_i, \mathbf{l}_j)$ to the nearest supported value within the estimated HDR; otherwise, set $\hat{d}(a_i, \mathbf{l}_j) = a_i$.
- Calculate

$$\hat{m}^{\text{feasible}}(a_i) = \frac{1}{n} \sum_{j=1}^n \hat{E}(Y | A = \hat{d}(a_i, \mathbf{l}_j), \mathbf{l}_j)$$

(c) **Trimming Estimand:**

- Estimate the trimming function:

$$\hat{t}(a_i, \mathbf{l}_j) = \begin{cases} \frac{1}{\hat{\tau}(a_i)}, & \text{if } \hat{f}(a_i | \mathbf{l}_j) \geq \hat{f}_\alpha^j, \\ 0, & \text{otherwise.} \end{cases}$$

- Calculate

$$\hat{m}^{\text{trimming}}(a_i) = \frac{1}{n} \sum_{j=1}^n \hat{E}(Y | A = a_i, \mathbf{l}_j) \cdot \hat{t}(a_i, \mathbf{l}_j)$$

6: Construct Compatibility Intervals (Optional):

- If using parametric or \sqrt{n} -consistent outcome models, and assuming standard regularity conditions, use the nonparametric bootstrap to construct approximate compatibility intervals for $\hat{m}^{\text{standard}}$, $\hat{m}^{\text{feasible}}$, and $\hat{m}^{\text{trimming}}$.

the methods in a more complex setting, incorporating multiple confounders and intricate data-generating processes.

4.1 Simulation Settings

4.1.1 Simulation 1: Correct model specification versus misspecification under positivity violations

We consider a simple scenario with a single time point where both the intervention and the confounder are normal-distributed shown in Appendix B.1. The simulation study involves three variations that share the same distribution for the confounder and intervention but differ in their outcome functions.

In Simulation 1A, the outcome function is linear. In Simulation 1B, the outcome function is sinusoidal, and in Simulation 1C, it is logarithmic. These two non-linear outcome functions in Simulations 1B and 1C pose a greater challenge for estimation, particularly in regions where data is sparse, i.e. suffering from positivity violations, leading to potential estimation difficulties. In contrast, the linear outcome function in Simulation 1A is expected to be easier to estimate, even in the presence of data sparsity, as the extrapolation will work perfectly.

The primary objective of this simulation design is to evaluate and compare the bias and variability in estimating both the standard CDRC, the proposed CDRC with most feasible intervention, and also the trimming estimand under conditions with positivity violations. This comparison provides insights into the strengths of the proposed most feasible intervention, particularly when outcome functions can not be reliably extrapolated.

4.1.2 Simulation 2: Correct model specification with positivity violations versus no positivity violations

We consider a different scenario with a single time point where the confounder is binary shown in Appendix B.2. The simulation study involves two variations that share the same distribution for the confounder and but differ in their intervention distribution.

In both variations, the intervention distributions given the confounder follow a truncated normal distribution with the same mean value conditional on L , but differ in variance. Simulation 2A has a lower variance, leading to greater deviation compared to Simulation 2B. Specifically, for $L = 0$ and $L = 1$, the overlap between the distributions of $A|L$ is minimal, indicating a higher degree of positivity violations, as shown in Figure 4a and 4b. The outcome function is a linear combination of A and L with a small noise term, making it straightforward to estimate and suitable for extrapolation.

The two simulations are designed to compare the estimation of the standard CDRC and the new estimands under conditions of positivity violations (2A) and no positivity violations (2B). This comparison will highlight the performance differences between the three estimands in scenarios where the positivity assumption is either met or violated.

4.1.3 Simulation 3: Simulation study in more complex setting inspired by real data

In this scenario, we consider a complex data-generating process, detailed in Appendix B.3. This process is inspired by real data from the CHAPAS-3 study, an open-label, parallel-group, randomized trial [26], which is further analyzed in Section 5 and follows the setup described in Schomaker et al. [31].

The outcome variable is binary and exhibits a non-linear relationship with the continuous intervention variable, which is modeled using a truncated normal distribution. The simulation aims to validate the proposed approaches in complex scenarios involving intricate distributions and diverse confounders with real-world significance.

4.2 Estimation and Evaluation

We set the sample size to $n = 1000$ for all simulation studies. The true value of each estimand m^ε , where $\varepsilon \in \{\text{standard, feasible, trimming}\}$, is computed by intervening on the data-generating process using the specified actions, with a large sample size of $N = 100,000$. For estimation (see Algorithm 1 for details), we apply

the parametric g-computation plug-in estimator in Simulations 1 and 2, and the HAL-based estimator in Simulation 3. The method for conditional density estimation varies by scenario: parametric linear regression (Simulation 1), nonparametric kernel methods (Simulation 2, using the R package `np` [12]), and Super Learner (Simulation 3; see Appendix C). We assess bias over $R = 1000$ Monte Carlo replications, defining absolute bias at level a as:

$$\text{Absolute Bias}(a) = \frac{1}{R} \sum_{r=1}^R |\hat{m}_r^\varepsilon(a) - m^\varepsilon(a)|.$$

with m^ε the true target parameter.

4.3 Results

The results of the simulations are summarized in Figures 3 to 5.

4.3.1 Simulation 1

Figure 3a illustrates the estimated conditional distribution and support levels at 50%, 90%, 95%, and 99%, overlaid with a scatter plot of observed data from a single simulation run. Areas outside these regions highlight rare combinations of L and Y in observation, reflecting data sparsity. Using the diagnostic approach from Section 2.2, we identify positivity violations, as shown in Figure 3b.

Figure 3b presents the non-overlap ratio, a diagnostic metric quantifying the proportion of the population for which specific interventions are infeasible at a 95% support level. This ratio, ranging from 0 to 1, reveals a clear pattern: in the central region, nearly all interventions have a non-overlap ratio of zero, indicating good feasibility. In contrast, the ratio rises sharply at the extremes, indicating that extremely small or large interventions are largely infeasible.

Together, Figures 3a and 3b show that certain interventions are rare or infeasible for subsets of the population. Even theoretically feasible, interventions may lack sufficient data for accurate estimation, underscoring the importance of our proposed feasible intervention framework.

Figure 3c examines the impact of non-overlap and model misspecification on the estimation of three estimands under linear, logarithmic, and sinusoidal outcome functions. In regions where the non-overlap ratio is near zero, counterfactual estimates for the three estimands are nearly identical across all outcome functions, as intended by the simulation design. At the extremes, however, the estimands diverge. The CDRC with the most feasible intervention establishes practical thresholds, avoiding unrealistic extrapolation into sparsely supported regions. The trimming estimand, by contrast, restricts the population to those for whom the intervention is feasible.

For linear outcome functions (Figure 3c, left), extrapolation is highly accurate, resulting in minimal absolute bias across all estimands (Figure 3d, left). However, for logarithmic and sinusoidal functions (Figure 3c, middle and right), extrapolation accuracy diminishes in sparsely supported regions, increasing absolute bias for all estimands (Figure 3d, middle and right).

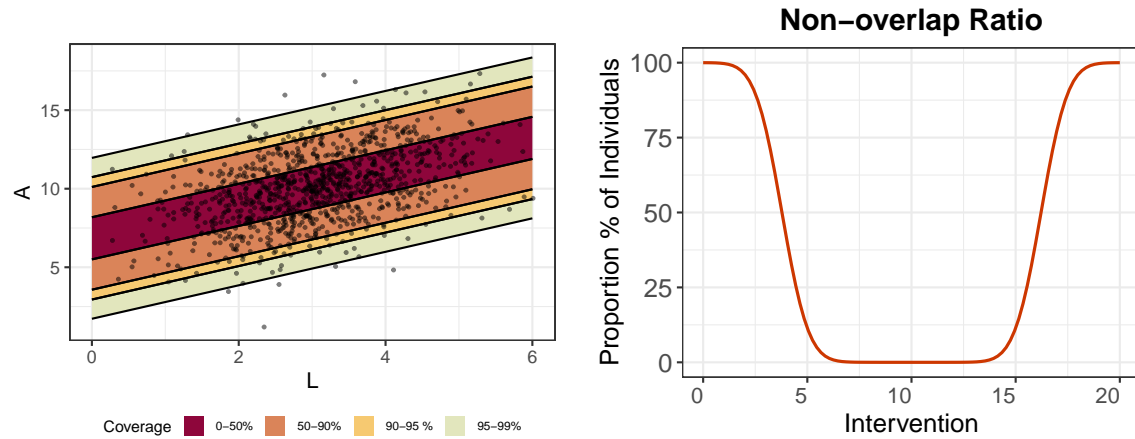
The most feasible intervention consistently achieves lower absolute bias, particularly when outcome functions are misspecified and extrapolation is unreliable. By focusing on well-supported regions, it avoids large biases and maintains robust estimates even in areas with low non-overlap. Conversely, the trimming estimand exhibits high variability and substantial absolute bias, even in the linear case, due to its restrictive population definition.

These results emphasize the benefits of the most feasible intervention approach, which balances estimation reliability and accuracy by limiting extrapolation only in feasible intervention regions.

4.3.2 Simulation 2

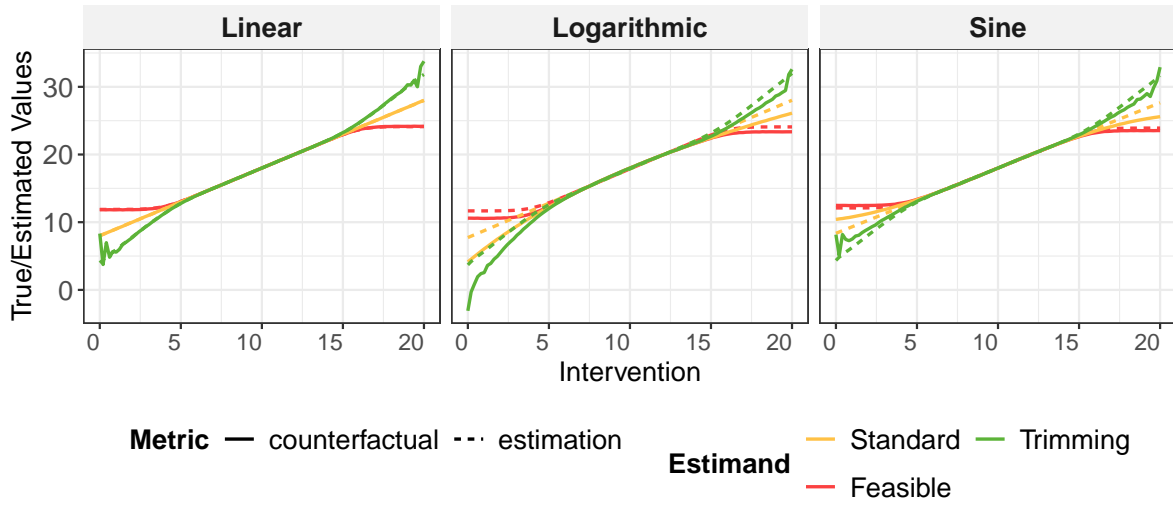
Figure 4a illustrates the conditional distribution of A given L . In Simulation 2A, this distribution is more concentrated, with lower variance compared to Simulation 2B. This distribution design increases the chance of non-overlap in Simulation 2B, as shown in Figure 4b.

Figure 4b presents the non-overlap ratio for each intervention. In Simulation 2B, the ratio is lower in the central region but rises sharply to 50% in the extreme intervention regions due to the divergence between

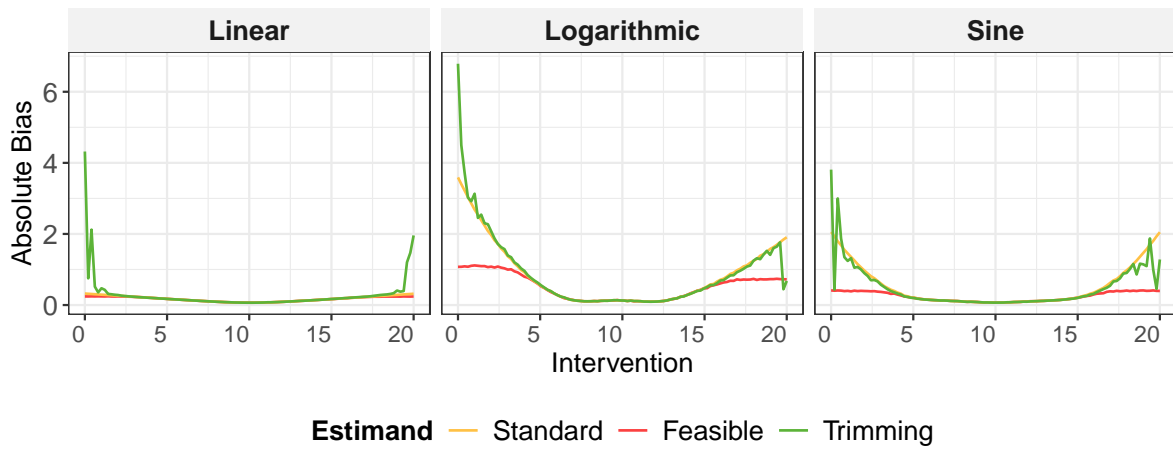


(a) Conditional density distribution of $A|L$ with different support level and scatter plot of observed data from one single simulation run.

(b) Non-overlap ratio: the conditional support with support level of 95%.

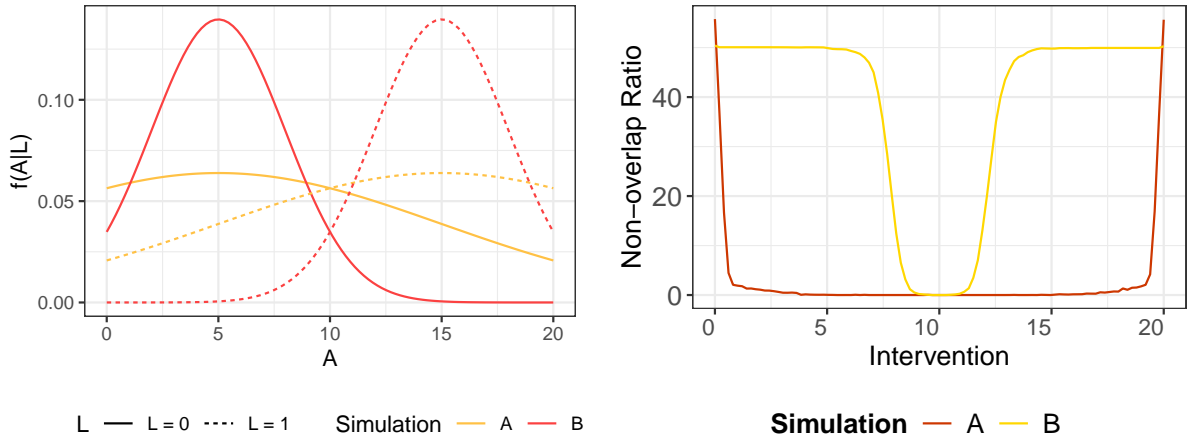


(c) Comparison of true and estimated values of m^{standard} , m^{feasible} , and m^{trimming} from Simulation 1. Separated by linear, logarithmic, and sinusoidal outcome functions across three simulation settings.



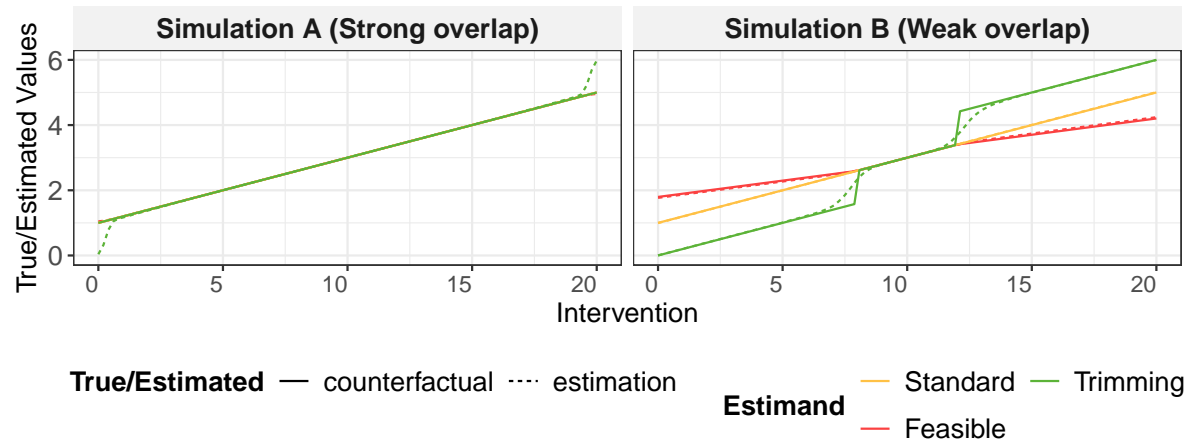
(d) Absolute bias of the estimation of m^{standard} , m^{feasible} , and m^{trimming} from Simulation 1. Separated by linear, logarithmic, and sinusoidal outcome functions across three simulation settings.

Figure 3: Results of Simulation 1

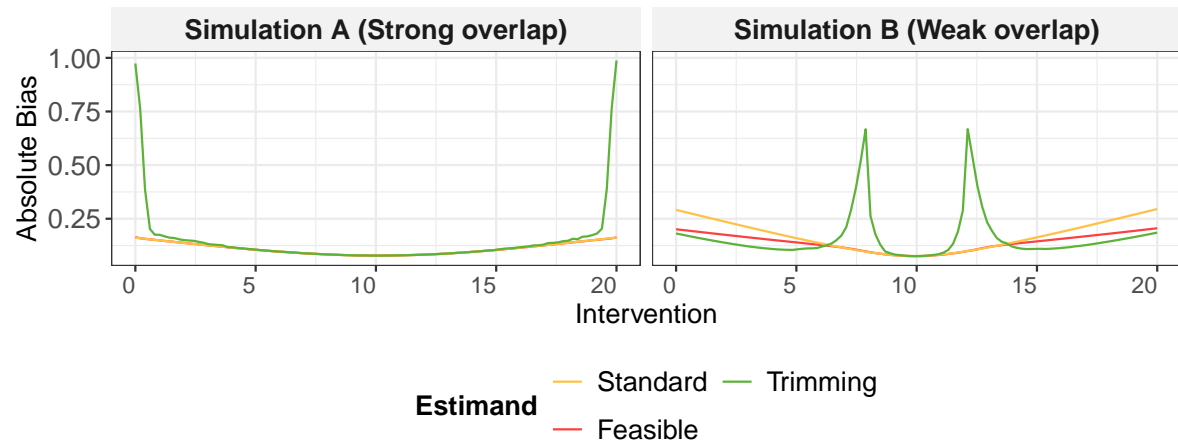


(a) True conditional density distribution of $A|L$ in simulation 2.

(b) Non-overlap ratio: the conditional support with support level of 95%.



(c) Comparison of true and estimated values of m^{standard} , m^{feasible} , and m^{trimming} from Simulation 2. Separated by Simulation 2A and 2B.



(d) Absolute bias of the estimation of m^{standard} , m^{feasible} , and m^{trimming} from Simulation 2. Separated by Simulation 2A and 2B.

Figure 4: Results of Simulation 2

the conditional distributions of A for $L = 0$ and $L = 1$. In contrast, Simulation 2A exhibits generally low non-overlap ratios across intervention values, except near the boundaries. This difference arises because, in Simulation 2B, the intervention distributions for $L = 0$ and $L = 1$ are distinct, whereas in Simulation 2A, they are more similar, exhibiting higher overlap.

Figure 4c shows the true estimand values for both the standard CDRC, the CDRC with the most feasible intervention and trimming estimand. In Simulation 2A, where non-overlap is absent, the three true curves are nearly identical because the intervention is feasible for all individuals. However, in Simulation 2B, the estimands diverge outside the central region, as the most feasible intervention shifts toward the center due to limited feasibility at extreme values, and the trimming estimand exhibits more radical counterfactual shifts. For all three curves, the estimates are very close to the true values, as the true outcome function is designed to be straightforward.

Figure 4d compares the absolute bias between Simulations 2A and 2B. Compared to Simulation 2A, Simulation 2B exhibits positivity violation issues, leading to higher absolute bias for all estimands, particularly in regions with high non-overlap. Nonetheless, the most feasible intervention shows lower bias under both conditions compared to the standard estimand and does not exceed the bias level of the standard estimand when positivity violations are minimal, as observed in Simulation 2A. The trimming estimand performs well at times, but it is unstable in certain areas.

4.3.3 Simulation 3

Figure 5a illustrates the non-overlap ratio in the range of $[0, 20]$, which shows a sharp increase at very low intervention values below 0.7 and above 10. In the following, we focus on the intervention region of $[0, 6]$.

Figure 5b presents the true and estimated values for the three estimands. In regions where the non-overlap ratio is zero, the three estimands are indistinguishable. However, the standard estimand increases dramatically near an intervention value of 0. As indicated by the non-overlap ratio, such values are nearly impossible to intervene on. In the data-generating process (see Appendix B.3), the truncated normal distribution excludes values below 0.2032, causing the true curve of the trimmed estimand to terminate near this intervention value. This indicates that intervention values below 0.2032 are strictly infeasible, representing a theoretical positivity violations and thus making counterfactual curve of trimming estimand unidentifiable below that threshold. Unlike the standard estimand, the proposed most feasible intervention estimand does not exhibit extreme values in regions with very low intervention, making it more robust and less prone to positivity issues.

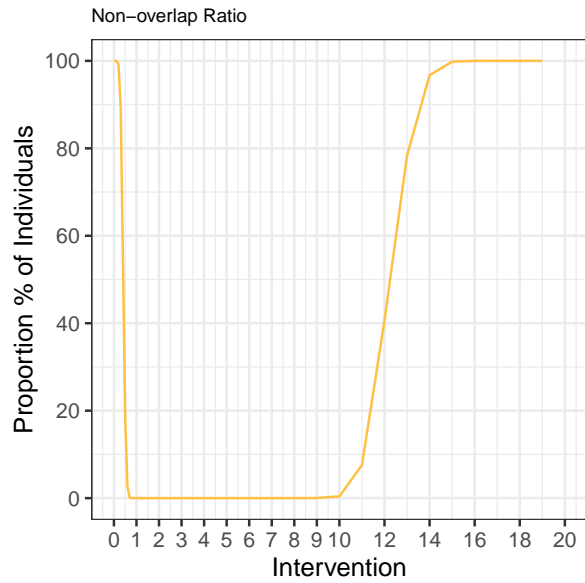
Figure 5c demonstrates that the most feasible intervention estimand consistently achieves lower absolute bias, particularly in regions with positivity violations. It effectively avoids large biases and maintains robust estimates even in areas with low or no non-overlap. While the trimming estimand also reduces bias, it becomes not estimable when the non-overlap ratio approaches 1, as no samples are available in such scenarios.

These findings underscore the practical utility of the proposed methods for complex data-generating processes with real-world significance.

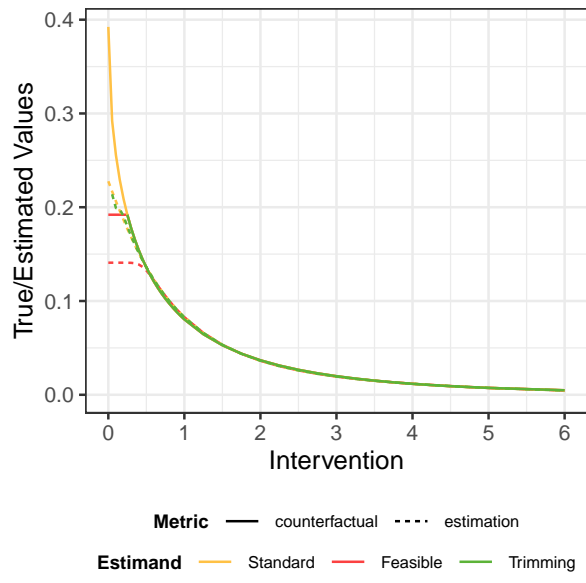
5 Data Analysis

We demonstrate our approach using pharmacoepidemiological data of HIV-positive children from the CHAPAS-3 trial, which enrolled children aged 1 month to 13 years in Zambia and Uganda [26, 1]. We focus on those 125 children who received efavirenz as part of antiretroviral therapy, together with both lamivudine and either stavudine, zidovudine, or abacavir.

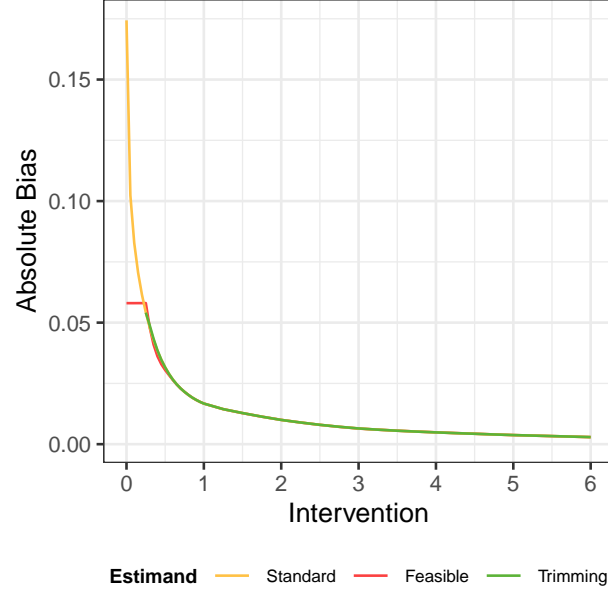
In line with previous studies [4, 5, 30], we are interested in how counterfactual viral failure probabilities (VL_t), defined as a viral load exceeding 100 copies/mL, vary as a function of different efavirenz concentrations (EFV_t , defined as the plasma concentration (in mg/L) measured 12 hours after dosing). Briefly, different patients who take the same efavirenz dose, may still have different drug concentrations in their blood, for example because of their individual metabolism. Patients exposed to suboptimal concentrations may experience negative outcomes and one may ask at which concentration level antiretroviral activity is too low to guarantee suppression for most patients. Thus, one may be interested in the concentration-response curve $a \mapsto P(VL^{EFV=a} = 1)$, $a \in [0, 6]$ mg/L; although it is known that not every child can achieve every possible



(a) Non-overlap ratio: the conditional support with support level of 95%.



(b) Comparison of true and estimated values of m^{standard} , m^{feasible} , and m^{trimming} from Simulation 3.



(c) Absolute bias of the estimation of m^{standard} , m^{feasible} , and m^{trimming} from Simulation 3.

Figure 5: Results of Simulation 3

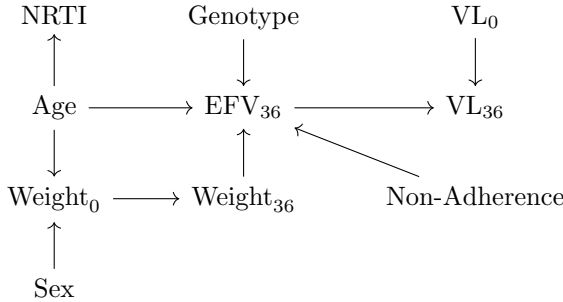


Figure 6: Directed acyclic graph (DAG) for CHAPAS-3 trial described in Section 5. NRTI refers to the Nucleoside Reverse Transcriptase Inhibitor drug component, sex, age, genotype relates to how fast the drug is cleared as determined by the 516G and 983T polymorphisms in the CYP2B6 gene [4], non-adherence describes any signs of non-adherence as measured through a medication event monitoring system [30] as well as weight. Subscripts describe the the week of measurement.

concentration level, depending on their clinical and metabolic profile and thus positivity violations may be likely [30].

For illustration, we use baseline data and data from the scheduled visit at $t = 36$ (weeks). The relevant part of the assumed data-generating process is, in line with previous studies [30, 18, 31], summarized by the directed acyclic graph (DAG) in Figure 6:

Our analysis illustrates the ideas based on a complete case analysis of all measured variables at $t = 36$ (weeks) represented in the DAG ($n = 83$). The analysis was conducted using three support levels for detecting non-overlap: 99%, 95%, and 90%. Our target estimand is the standard causal concentration-response curve, defined in Section 3.1. We compare this estimand to the proposed estimand with most feasible intervention strategy, described in Section 3.3.3, as well as the trimming estimand in Section 3.3.4. The estimation process closely follows the detailed methodology described in Section 3.4 and algorithm outlined in Algorithm 1. Note: To quantify uncertainty, obtaining reliable compatibility intervals is challenging in this setting, both because the functional parameter defined in Equation (16) is not pathwise differentiable and because of uncertainty around ideal model specification. Since bootstrap inference may be unreliable in such nonregular problems, we report only point estimates in the application and acknowledge this limitation.

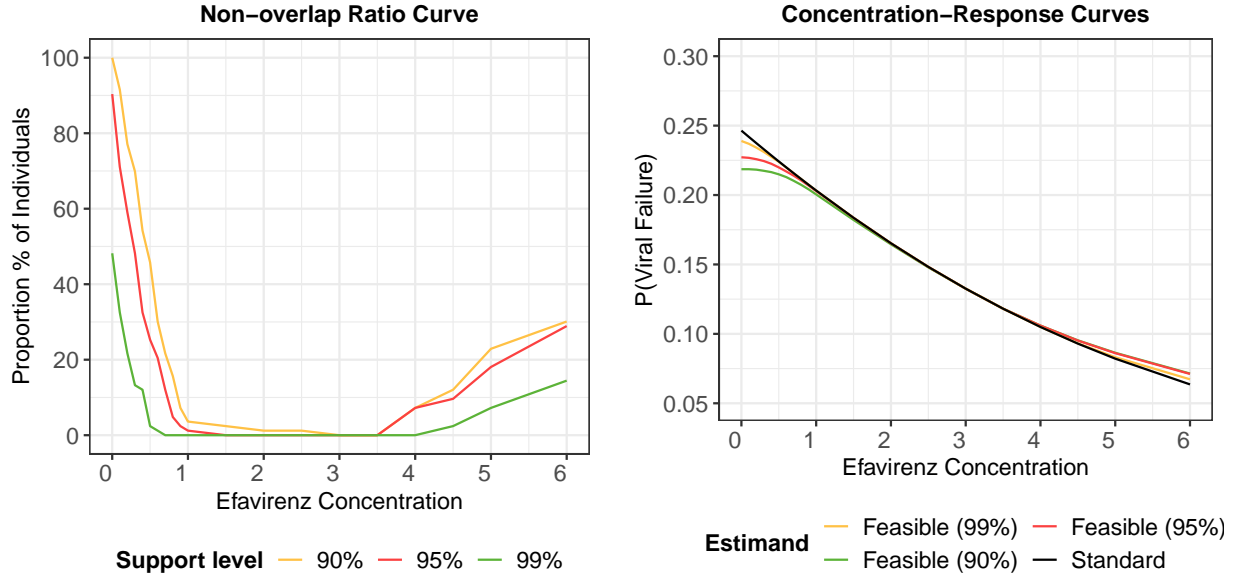
5.1 Results

The results of the analysis are presented in Figure 7 and are discussed in two parts: (1) diagnostics assessing the extent of positivity violations based on intervention values, and (2) estimates of three estimands.

Figure 7a illustrates the proposed non-overlap ratios as diagnostics for identifying positivity violations in continuous interventions. These ratios, calculated as a function of the intervention EFV_{36} , represent the proportion of the population where the intervention is not feasible, based on 3 support levels of non-overlap detection.

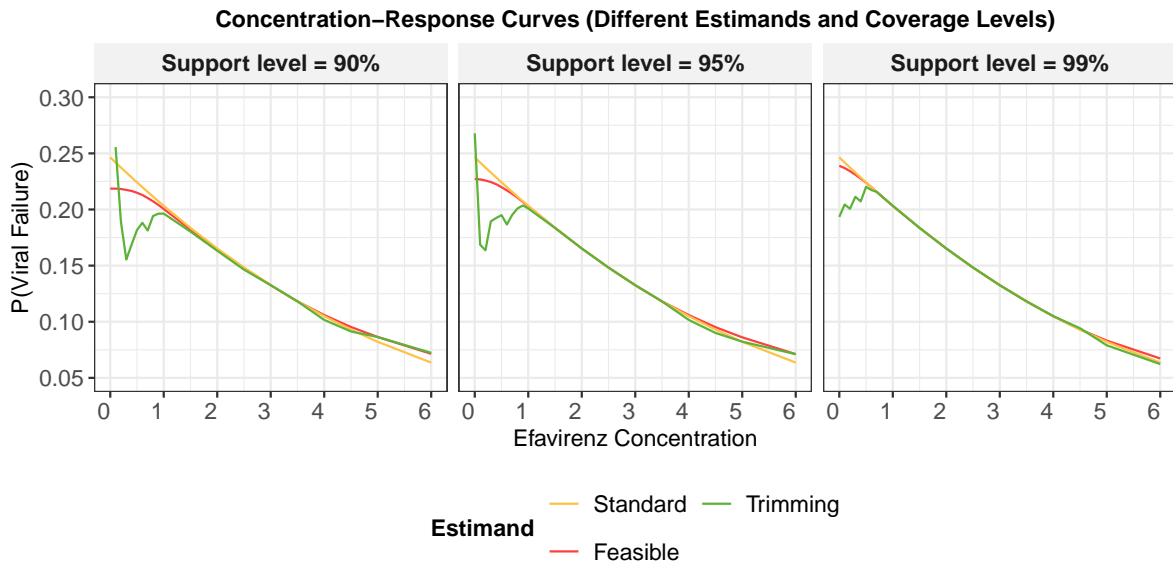
The non-overlap ratios remain low across all support levels within the central intervention range (approximately 1 to 3.5 mg/L), suggesting minimal violations of positivity in this region and supporting reliable causal estimation. However, at the boundaries of the intervention range—below 1 mg/L or above 3.5 mg/L—the ratios increase, indicating more frequent violations. Notably, near 0 mg/L, the non-overlap ratio rises sharply, signaling strong violations of the positivity assumption, consistent with the fact that concentrations this low are virtually impossible to observe.

Figure 7b show the estimated curves of the most feasible intervention across three support levels compared with the standard causal concentration-response curve. In regions with positivity violations, using the most feasible intervention strategy differs from the CDRC, while closely aligning with standard estimates in well-supported regions. This means whenever a concentration value seems unlikely or implausible, we do not enforce this intervention but rather use the closest value that is possible. This may happen, for example, if there are patients with a very slow metabolism who will never be able to clear the drug fast enough to ever achieve concentrations under 1 mg/L.



(a) Non-overlap ratio at support level of 90%, 95% and 99%. As the support level increases, there is greater tolerance for non-overlap detection. Major positivity violations occur in intervention regions with values below 1 and above 3.5.

(b) Comparison of different curves including feasible interventions with support level 90%, 95% and 99%, and the standard curve.



(c) Comparison with of different curves. Separated by support level of 90%, 95% and 99%.

Figure 7: Results of the data analysis

Figure 7c compares all estimated causal curves across three support levels. As the support level increases, more positivity violations are tolerated for both the feasible intervention and trimming estimands. However, the trimming estimand exhibits instability in regions with strong positivity violations, suggesting that it may not be the optimal approach in this analysis.

6 Discussion

6.1 Summary

Positivity violations are a persistent challenge in causal inference with continuous interventions, particularly when outcome regressions must be extrapolated from observed to unobserved regions. Such violations arise when certain intervention levels are insufficiently represented in the data, undermining both the identification and estimation of causal effects.

We address this challenge with a data-adaptive framework that employs an L -specific density threshold f_α to define highest density regions $\mathcal{A}_\alpha(\mathbf{l})$. Conceptually, this idea is related to Modified Treatment Policies (MTPs), since both approaches avoid assigning interventions to strata with poor support. The objectives, however, differ: MTPs define modified treatment (often based on natural values) to ensure feasibility, whereas our method preserves the causal dose-response curve (CDRC) as much as possible. As Ring et al. [28] note, even MTPs may not fully resolve positivity violations when the modified treatment lacks adequate support.

Our approach also contrasts with the weighted CDRC proposed by Schomaker et al. [31]. Both approaches address positivity violations via conditional densities, but they differ in how the estimand is adapted. First, we employ a unit-specific, data-adaptive threshold, whereas Schomaker et al. use a fixed cutoff c , which may be unsuitable across intervention ranges and covariate strata. Second, our framework serves dual purposes: it functions both as a diagnostic tool (see Section 2.3) and as a procedure for defining a feasible intervention rule. A further distinction lies in interpretability. Our method modifies intervention assignments explicitly (to the “closest feasible” value) and targets the clearly defined quantity $E(Y^d)$. In contrast, the weighted CDRC redefines the estimand implicitly through a projection within the expectation, thereby changing the target parameter.

Suppose, for example, that $\hat{f}(0.5 \mid \text{adherent, slow metabolizer}) \approx 0$, indicating that assigning treatment $a = 0.5$ is biologically implausible for that stratum. The weighted CDRC of Schomaker et al. addresses this not by extrapolating the outcome model into unsupported regions, but by *redefining the target* at a through a projection that downweights such strata. The identified parameter coincides with the standard causal curve in well-supported strata $\{f(a \mid \mathbf{l}) > c\}$, while replacing contributions from unsupported strata $\{f(a \mid \mathbf{l}) \leq c\}$ with a weighted associational term. In this example, the (adherent, slow metabolizer) group contributes negligibly at $a = 0.5$ because $f(0.5 \mid \mathbf{l}) \approx 0$; identifiability is thus preserved without extrapolation. The trade-off is that $m^{\text{weighted}}(a)$ no longer corresponds to a clear assignment target such as $\mathbb{E}(Y^a)$ or $\mathbb{E}(Y^d)$: it blends the causal curve where support exists with a projection-based contribution elsewhere, thereby shifting the scientific estimand and reducing interpretability while gaining identifiability. By contrast, our method substitutes infeasible interventions with a transparent, data-driven rule, preserving both identifiability and causal interpretability.

A key consequence of positivity violations is increased estimation bias—even when models are correctly specified—because estimation relies on extrapolation into unsupported regions. The issue is therefore not merely one of model misspecification but one of fundamental identifiability. Our data-adaptive intervention framework addresses this challenge by reassigning infeasible interventions to regions with adequate empirical support, thereby avoiding extrapolation and ensuring more reliable estimation.

6.2 Limitations

Estimating the full CDRC under continuous interventions faces several fundamental limitations. First, under mild smoothness conditions, the CDRC is non-pathwise differentiable [8]. This rules out the use of influence-function-based estimators such as TMLE or doubly robust procedures, unless additional structural assumptions are imposed. While some recent approaches achieve robustness by assuming differentiability [22], monotonicity [36], or smooth invertibility [9], such assumptions may be difficult to defend in applied contexts

where the estimand is determined by the scientific question. Thus, double robustness and semiparametric efficiency are generally unattainable in this setting.

Second, the data-adaptive nature of our proposed intervention introduces dependence between the observed data and the estimand. As noted by Hubbard et al. [19], this dependence violates standard independence assumptions and may compromise the validity of inference procedures such as the bootstrap. Sample splitting or cross-validation can help restore approximate independence by separating the construction of the data-adaptive intervention rule from estimation of the target parameter, but these remedies introduce practical complexity: they yield multiple, split-specific estimands and complicate interpretability.

Third, the performance of our approach depends on the stability of the data-adaptive rule itself. In particular, the choice of the support level α , the method for estimating highest density regions, and the specification of the substitution function all influence the resulting estimand. Instability in these components may introduce variability or sensitivity in finite samples, raising concerns about robustness and reproducibility across different applications.

In light of these challenges, our work pursues a complementary goal: preserving the original CDRC estimand while addressing positivity violations through data-adaptive interventions. This yields a natural plug-in estimator that avoids extrapolation and provides valid inference under correct model specification, provided the data-adaptive rule is reasonably stable. Although our approach does not deliver double robustness, it enhances interpretability and resilience to misspecification by focusing estimation on well-supported regions. To evaluate the impact of data-adaptivity on inference, we conducted a simulation study (Appendix D) comparing bootstrap coverage with and without sample splitting. The results suggest that, in well-supported regions, bootstrap intervals remain reasonably accurate even without splitting.

Finally, although our method provides a principled approach for substituting infeasible interventions with their most feasible counterparts—thereby preserving fidelity to the standard CDRC and enhancing interpretability—important avenues remain for future work. In particular, further research is needed to extend the framework to longitudinal settings, refine the design of substitution rules, and develop more robust techniques for estimating support regions, especially in high-dimensional and complex treatment spaces.

Acknowledgments

We sincerely thank the CHAPAS-3 trial team for their support, valuable advice on the illustrative data analysis, and for providing access to their data.

We extend our special thanks to Sarah Walker, Di Gibb, Andrzej Bienczak, David Burger, Elizabeth Kaudha, Paolo Denti, and Helen McIlheron for valuable advice regarding the data and continuous support. Additionally, we are deeply grateful to Iván Díaz for his constructive and insightful feedback on earlier versions of this manuscript.

The research is supported by the German Research Foundations (DFG) Heisenberg Program (grants 465412241 and 465412441).

References

- [1] G. Abongomera, A. Cook, V. Musiime, C. Chabala, M. Lamorde, J. Abach, M. Thomason, V. Mulenga, A. Kekitiinwa, R. Colebunders, C. Kityo, A. S. Walker, D. M. Gibb, and CHAPAS-3 Trial Team. Improved adherence to antiretroviral therapy observed among hiv-infected children whose caregivers had positive beliefs in medicine in sub-saharan africa. *Aids and Behavior*, 21(2):441–449, 2017.
- [2] David Benkeser and Mark Van Der Laan. The highly adaptive lasso estimator. In *2016 IEEE international conference on data science and advanced analytics (DSAA)*, pages 689–696. IEEE, 2016.
- [3] Peter J Bickel and David A Freedman. Some asymptotic theory for the bootstrap. *The annals of statistics*, 9(6):1196–1217, 1981.
- [4] Andrzej Bienczak, Paolo Denti, Adrian Cook, Lubbe Wiesner, Veronica Mulenga, Cissy Kityo, Addy Kekitiinwa, Diana M Gibb, David Burger, A Sarah Walker, et al. Plasma efavirenz exposure, sex, and

age predict virological response in hiv-infected african children. *JAIDS Journal of Acquired Immune Deficiency Syndromes*, 73(2):161–168, 2016.

[5] Andrzej Bienczak, Paolo Denti, Adrian Cook, Lubbe Wiesner, Veronica Mulenga, Cissy Kityo, Addy Kekitiinwa, Diana M Gibb, David Burger, Ann S Walker, et al. Determinants of virological outcome and adverse events in african children treated with paediatric nevirapine fixed-dose-combination tablets. *Aids*, 31(7):905–915, 2017.

[6] Zachary Butzin-Dozier, Sky Qiu, Alan E. Hubbard, Junming (Seraphina) Shi, and Mark J. van der Laan. Highly adaptive lasso: Machine learning that provides valid nonparametric inference in realistic models. *medRxiv*, 2024. doi: 10.1101/2024.10.18.24315778. URL <https://www.medrxiv.org/content/early/2024/10/19/2024.10.18.24315778>.

[7] Richard K Crump, V Joseph Hotz, Guido W Imbens, and Oscar A Mitnik. Dealing with limited overlap in estimation of average treatment effects. *Biometrika*, 96(1):187–199, 2009.

[8] Iván Díaz and Mark J van der Laan. Targeted data adaptive estimation of the causal dose–response curve. *Journal of Causal Inference*, 1(2):171–192, 2013.

[9] Iván Díaz, Nicholas Williams, Katherine L Hoffman, and Edward J Schenck. Nonparametric causal effects based on longitudinal modified treatment policies. *Journal of the American Statistical Association*, 118(542):846–857, 2023.

[10] Iván Díaz Muñoz and Mark J van der Laan. Super learner based conditional density estimation with application to marginal structural models. *The international journal of biostatistics*, 7(1):0000102202155746791356, 2011.

[11] Sebastian Haneuse and Andrea Rotnitzky. Estimation of the effect of interventions that modify the received treatment. *Statistics in medicine*, 32(30):5260–5277, 2013.

[12] Tristen Hayfield and Jeffrey S Racine. Nonparametric econometrics: The np package. *Journal of statistical software*, 27:1–32, 2008.

[13] Nima S Hejazi, David Benkeser, Iván Díaz, and Mark J van der Laan. Efficient estimation of modified treatment policy effects based on the generalized propensity score. 2022. URL <https://arxiv.org/abs/2205.05777>.

[14] Nima S Hejazi, David C Benkeser, and Mark J van der Laan. *haldensify: Highly adaptive lasso conditional density estimation*, 2022. URL <https://doi.org/10.5281/zenodo.3698329>. R package version 0.2.5.

[15] Nima S Hejazi, Mark J van der Laan, and David Benkeser. haldensify: Highly adaptive lasso conditional density estimation inr. *Journal of Open Source Software*, 7(77):4522, 2022.

[16] Nima S Hejazi, Mark J van der Laan, and David C Benkeser. haldensify: Highly adaptive lasso conditional density estimation in R. *Journal of Open Source Software*, 2022. doi: 10.21105/joss.04522. URL <https://doi.org/10.21105/joss.04522>.

[17] Miguel A Hernán and James M Robins. *Causal inference: What if*. Boca Raton: Chapman & Hall/CRC, 2020.

[18] A. Holovchak, H. McIlleron, P. Denti, and M. Schomaker. Recoverability of causal effects in a longitudinal study under presence of missing data. *Biostatistics*, in press, <https://arxiv.org/abs/2402.14562>, 2024.

[19] Alan E Hubbard, Sara Kherad-Pajouh, and Mark J Van Der Laan. Statistical inference for data adaptive target parameters. *The international journal of biostatistics*, 12(1):3–19, 2016.

[20] Rob J Hyndman. Computing and graphing highest density regions. *The American Statistician*, 50(2):120–126, 1996.

[21] Guido W Imbens and Donald B Rubin. *Causal inference for statistics, social, and biomedical sciences: An introduction*. Cambridge University Press, 2015.

[22] Edward H Kennedy, Zongming Ma, Matthew D McHugh, and Dylan S Small. Non-parametric methods for doubly robust estimation of continuous treatment effects. *Journal of the Royal Statistical Society Series B: Statistical Methodology*, 79(4):1229–1245, 2017.

[23] Michael R Kosorok. *Introduction to empirical processes and semiparametric inference*. Springer, 2008.

[24] Maxime Léger, Arthur Chatton, Florent Le Borgne, Romain Pirracchio, Sigismond Lasocki, and Yohann Foucher. Causal inference in case of near-violation of positivity: comparison of methods. *Biometrical Journal*, 64(8):1389–1403, 2022.

[25] Chiara Moccia, Giovenale Moirano, Maja Popovic, Costanza Pizzi, Piero Fariselli, Lorenzo Richiardi, Claus Thorn Ekstrøm, and Milena Maule. Machine learning in causal inference for epidemiology. *European Journal of Epidemiology*, pages 1–12, 2024.

[26] Veronica Mulenga, Victor Musiime, Adeodata Kekitiinwa, Adrian D. Cook, George Abongomera, Julia Kenny, Chisala Chabala, Grace Mirembe, Alice Asiimwe, Ellen Owen-Powell, David Burger, Helen McIlleron, Nigel Klein, Chifumbe Chintu, Margaret J. Thomason, Cissy Kityo, A. Sarah Walker, Diana M. Gibb, and Chapas-trial team. Abacavir, zidovudine, or stavudine as paediatric tablets for african hiv-infected children (chapas-3): an open-label, parallel-group, randomised controlled trial. *The Lancet Infectious diseases*, 16(2):169–79, 2016.

[27] Maya L Petersen, Kristin E Porter, Susan Gruber, Yue Wang, and Mark J Van Der Laan. Diagnosing and responding to violations in the positivity assumption. *Statistical methods in medical research*, 21(1):31–54, 2012.

[28] Katharina Ring and Michael Schomaker. A diagnostic to find and help combat positivity issues—with a focus on continuous treatments. *arXiv preprint arXiv:2502.11820*, 2025.

[29] Donald B Rubin. Estimating causal effects of treatments in randomized and nonrandomized studies. *Journal of educational Psychology*, 66(5):688, 1974.

[30] M. Schomaker, P. Denti, A. Bienczak, D. Burger, I. Diaz, D. Gibb, S. Walker, and H. McIlleron. Determining targets for antiretroviral drug concentrations: a causal framework illustrated with pediatric efavirenz data from the CHAPAS-3 trial. *Pharmacoepidemiology and Drug Safety*, in press, 2024.

[31] M. Schomaker, H. McIlleron, P. Denti, and I. Diaz. Causal inference for continuous multiple time point interventions. *Statistics in Medicine*, 43(28):5380–5400, 2024.

[32] Junming Shi, Wenxin Zhang, Alan E Hubbard, and Mark van der Laan. Hal-based plugin estimation of the causal dose-response curve. *arXiv preprint arXiv:2406.05607*, 2024.

[33] Mark van der Laan. Higher order spline highly adaptive lasso estimators of functional parameters: Pointwise asymptotic normality and uniform convergence rates. *arXiv preprint arXiv:2301.13354*, 2023.

[34] Aad W Van der Vaart. *Asymptotic statistics*, volume 3. Cambridge university press, 2000.

[35] Aad W Van Der Vaart and Jon A Wellner. Weak convergence. In *Weak convergence and empirical processes: with applications to statistics*, pages 16–28. Springer, 1996.

[36] Ted Westling, Peter Gilbert, and Marco Carone. Causal isotonic regression. *Journal of the Royal Statistical Society Series B: Statistical Methodology*, 82(3):719–747, 2020.

[37] Daniel Westreich and Stephen R Cole. Invited commentary: positivity in practice. *American journal of epidemiology*, 171(6):674–677, 2010.

[38] Paul N Zivich, Stephen R Cole, and Daniel Westreich. Positivity: Identifiability and estimability. *arXiv preprint arXiv:2207.05010*, 2022.

[39] Paul N Zivich, Rachael K Ross, Bonnie E Shook-Sa, Stephen R Cole, and Jessie K Edwards. Empirical sandwich variance estimator for iterated conditional expectation g-computation. *Statistics in Medicine*, 43(29):5562–5572, 2024.

A Additional Information

In the literature, positivity violations are typically classified into two types—structural and practical—usually in the context of binary interventions [38, 27, 37]. Analogous definitions can be formulated for continuous interventions.

A.1 Near positivity violations

Near violations occur when the positivity assumption is almost, but not completely, violated. Here, the probability of receiving certain treatment levels given specific confounder combinations is very close to zero but not exactly zero. Although not a strict violation, the consequences are similar: bias and loss of precision in causal estimation [24]. Estimators become unstable in these regions, since causal methods are particularly sensitive to sparse data [24].

A.2 Structural positivity violations

Structural violations arise when, due to the design or data structure, some subgroups of individuals (defined by their confounders) have no chance of receiving certain treatment values. Formally, $f_{A|\mathbf{L}}(a|\mathbf{L}) = 0$ for these combinations.

A.3 Practical positivity violations

Also called stochastic violations, these occur when a treatment is clinically possible for some confounder strata but is unobserved in the data, leading to $\hat{f}_{A|\mathbf{L}}(a|\mathbf{L}) = 0$. For continuous interventions this notion is more subtle: exact intervention values are never observed, so whether $\hat{f}(a|\mathbf{L}) = 0$ depends on how the conditional density is estimated.

A.4 Theoretical implications for plug-in estimation

Positivity violations—whether structural (deterministic absence of support) or practical (sparse data)—create fundamental difficulties for plug-in estimation of the causal dose-response curve (CDRC) in Equation 6. To formalize these issues, let

$$Q_0(a, \mathbf{l}) := E_{P_0}(Y \mid A = a, \mathbf{L} = \mathbf{l})$$

denote the true conditional outcome regression. Under standard identification assumptions, the CDRC is identified by the g-formula:

$$m(a) = E_{P_0}[Q_0(a, \mathbf{L})]. \quad (21)$$

Step 1: Estimation of the regression function.

In practice, one estimates $Q_0(a, \mathbf{l}) = E_{P_0}(Y \mid A = a, \mathbf{L} = \mathbf{l})$ by fitting a regression function $\hat{Q}(A, \mathbf{L})$, for example via least squares. The corresponding population risk of a candidate function Q is

$$R(Q) = E_{P_0}[(Y - Q(A, \mathbf{L}))^2]. \quad (22)$$

By the variance decomposition identity,

$$R(Q) = E_{P_0}[(Q_0(A, \mathbf{L}) - Q(A, \mathbf{L}))^2] + E_{P_0}[\text{Var}(Y \mid A, \mathbf{L})].$$

Since the second term does not depend on Q , minimizing (22) is equivalent to minimizing

$$\int (Q_0(A, \mathbf{L}) - Q(A, \mathbf{L}))^2 dP_{A, \mathbf{L}}. \quad (23)$$

Thus, estimation implicitly weights squared errors by the observed joint density $f_{A,\mathbf{L}}(a, \mathbf{l}) = f_{A|\mathbf{L}}(a | \mathbf{l}) f_{\mathbf{L}}(\mathbf{l})$. Equivalently, the contribution of a given stratum \mathbf{l} to the risk is scaled by its marginal probability $f_{\mathbf{L}}(\mathbf{l})$, and within each stratum the influence of treatment level a is weighted by its conditional density $f_{A|\mathbf{L}}(a | \mathbf{l})$. Hence, regions with low support (small $f_{A|\mathbf{L}}(a | \mathbf{l})$) contribute negligibly to the risk, and therefore exert little influence on the fitted regression \hat{Q} .

Step 2: Plug-in estimation of the CDRC.

The plug-in estimator of (21) is

$$\hat{m}(a) = E_{P_n} [\hat{Q}(a, \mathbf{L})],$$

where P_n is the empirical distribution of \mathbf{L} and \hat{Q} is the fitted regression. Its mean squared error decomposes as

$$\text{MSE}(\hat{m}(a)) = E_{P_0} \left[(\hat{Q}(a, \mathbf{L}) - Q_0(a, \mathbf{L}))^2 \right] = \int (\hat{Q}(a, \mathbf{l}) - Q_0(a, \mathbf{l}))^2 dP_{\mathbf{L}}(\mathbf{l}). \quad (24)$$

The mismatch:

Equations (22) and (24) highlight a fundamental mismatch:

- The regression step minimizes loss with respect to $P_{A,\mathbf{L}}$, effectively weighting errors by $f_{A|\mathbf{L}}(a | \mathbf{l}) f_{\mathbf{L}}(\mathbf{l})$.
- The target parameter averages errors with respect to the marginal distribution $P_{\mathbf{L}}$, so that each stratum contributes in proportion to its prevalence in the population, regardless of whether the treatment level $A = a$ is well supported in that stratum.

Formally, the regression risk is

$$R(g) = \int (Q_0(a, \mathbf{l}) - g(a, \mathbf{l}))^2 f_{A|\mathbf{L}}(a | \mathbf{l}) f_{\mathbf{L}}(\mathbf{l}) da d\mathbf{l},$$

whereas the CDRC error criterion is

$$\text{MSE}(\hat{m}(a)) = \int (Q_0(a, \mathbf{l}) - \hat{Q}(a, \mathbf{l}))^2 f_{\mathbf{L}}(\mathbf{l}) d\mathbf{l}.$$

Thus, if $f_{A|\mathbf{L}}(a | \mathbf{l}) \approx 0$, errors in approximating $Q_0(a, \mathbf{l})$ are essentially ignored when fitting \hat{Q} , but those same errors can dominate the plug-in bias in (24) because they are weighted by $f_{\mathbf{L}}(\mathbf{l})$ rather than $f_{A|\mathbf{L}}(a | \mathbf{l})$.

Implication. This discrepancy explains why plug-in g-computation is highly sensitive to positivity violations. Even if the regression is consistent in regions with support, small errors in sparse or unsupported strata—where extrapolation is unavoidable—are not controlled by the empirical risk but nevertheless contribute directly to bias in $\hat{m}(a)$.

B Simulation Parameters

B.1 Data Generating Process for Simulation 1

$$\begin{aligned} L &\sim N(\mu = 3, \sigma = 1) \\ A &\sim N(\mu = 10 + 0.7 \cdot L, \sigma = 3) \end{aligned}$$

B.1.1 Simulation 1A: Linear outcome function

$$Y \sim N(\mu = 10 + A + 0.5 \cdot L, \sigma = 3)$$

B.1.2 Simulation 1B: Sinusoidal outcome function

$$Y \sim N \left(\mu = 10 + 10 \cdot \sin \left(\frac{A - 10}{10} \right) + 0.5 \cdot L, \sigma = 3 \right)$$

B.1.3 Simulation 1C: Logarithmic outcome function

$$Y \sim N \left(\mu = 10 + 30 \cdot \log \left(\frac{A - 10}{30} \right) + 0.5 \cdot L, \sigma = 3 \right)$$

B.2 Data Generating Process for Simulation 2

$$L \sim \text{Bernoulli}(p = 0.5)$$

B.2.1 Simulation 2A

$$\begin{aligned} A|L &\sim \mathcal{N}_{\text{trunc}}(\mu = 10 + 5 \cdot L, \sigma = 3, l = 0, h = 20, \\ &\quad l_a = h_a = 0, l_b = h_b = 20) \\ Y|A, L &\sim N(\mu = 0.05 \cdot A + 0.5 \cdot L, \sigma = 2) \end{aligned}$$

B.2.2 Simulation 2B

$$\begin{aligned} A|L &\sim \mathcal{N}_{\text{trunc}}(\mu = 10 + 5 \cdot L, \sigma = 10, l = 0, h = 20, \\ &\quad l_a = h_a = 0, l_b = h_b = 20) \\ Y|A, L &\sim N(\mu = 0.05 \cdot A + 0.5 \cdot L, \sigma = 2) \end{aligned}$$

B.3 Data Generating Process for Simulation 3

$$\text{Sex} \sim \text{Bernoulli}(p = 0.5)$$

Genotype \sim Categorical

$$p = \begin{cases} \text{logit}^{-1}(-0.103 + \text{Sex} \cdot 0.223 + (1 - \text{Sex}) \cdot 0.173), \\ \text{logit}^{-1}(-0.086 + \text{Sex} \cdot 0.198 + (1 - \text{Sex}) \cdot 0.214), \\ \text{logit}^{-1}(-0.309 + \text{Sex} \cdot 0.082 + (1 - \text{Sex}) \cdot 0.107) \end{cases}$$

$$\begin{aligned} \text{Age} &\sim \mathcal{N}_{\text{trunc}}(\mu = 1.501, \sigma = 0.369, l = 0.693, h = 2.8, \\ &\quad l_a = 0.693, l_b = 1, h_a = 1, h_b = 2.8) \end{aligned}$$

$$\begin{aligned} \text{Weight}_0 &\sim \mathcal{N}_{\text{trunc}}(\mu = 1.5 + 0.2 \cdot \text{Sex} + 0.774 \cdot \text{Age}, \\ &\quad \sigma = 0.3, l = 2.26, h = 3.37, \\ &\quad l_a = 2.26, l_b = 2.67, h_a = 3.02, h_b = 3.37) \end{aligned}$$

NRTI \sim Categorical

$$p = \begin{cases} \text{logit}^{-1}(-0.006 + \text{Age} \cdot (0.1735 \cdot \mathbb{1}_{\{\text{Age} > 1.4563\}} + 0.157)) \\ \text{logit}^{-1}(-0.006 + \text{Age} \cdot (0.1570 \cdot \mathbb{1}_{\{\text{Age} > 1.4563\}} + 0.1818)) \end{cases}$$

$$\text{CoMo}_0 \sim \text{Bernoulli}(p = 0.15)$$

Dose₀ \sim Categorical

$$p = \begin{cases} \text{logit}^{-1}(5 + 8 \cdot \sqrt{\text{Weight}_0} - 10 \cdot \text{Age}) \\ \text{logit}^{-1}(4 + 8.768 \cdot \sqrt{\text{Weight}_0} - 9.060 \cdot \text{Age}) \\ \text{logit}^{-1}(3 + 6.562 \cdot \sqrt{\text{Weight}_0} - 8.325 \cdot \text{Age}) \end{cases}$$

$$\begin{aligned} \text{EFV}_0 &\sim \mathcal{N}_{\text{trunc}}(\mu = -8 + 0.1 \cdot \text{Age} + 4.66 \cdot \text{Genotype} \\ &\quad + 0.1 \cdot \text{Dose}_0 + 2.66 \cdot \mathbb{1}_{\{\text{Genotype} \leq 2\}} \\ &\quad + 4.6 \cdot \mathbb{1}_{\{\text{Genotype} = 3\}}, \sigma = 4.06, l = 0.2032, h = 21, \\ &\quad l_a = 0.2032, l_b = 0.88, h_a = 8.376, h_b = 21) \end{aligned}$$

$$\begin{aligned} \text{VL}_0 &\sim \text{Bernoulli}(p = 1 - \text{logit}^{-1}(0.4 \\ &\quad + 1.9 \cdot \sqrt{\text{EFV}_0})) \end{aligned}$$

$$\begin{aligned} \text{MEMS} &\sim \text{Bernoulli}(p = \text{logit}^{-1}(0.31 \cdot \text{CoMo}_0 \\ &\quad + 0.71)) \end{aligned}$$

$$\begin{aligned} \text{Weight} &\sim \mathcal{N}_{\text{trunc}}(\mu = -0.05 \cdot \mathbb{1}_{\{\text{CoMo}_0 = 1\}} + 1.04 \cdot \text{Weight}_0, \\ &\quad \sigma = 0.4, l = 2.26, h = 3.37, \\ &\quad l_a = 2.26, l_b = 2.473, h_a = 3.2, h_b = 3.37) \end{aligned}$$

$$\begin{aligned}
\text{CoMo} &\sim \text{Bernoulli}(p = 1 - \text{logit}^{-1}(0.5 \cdot \mathbb{1}_{\{\text{CoMo}_0=1\}} \\
&\quad + 0.1 \cdot \text{Age} + 0.1 \cdot \text{Weight}_0)) \\
\text{Dose} &\sim \text{Categorical} \\
p &= \begin{cases} \text{logit}^{-1}(4 + 0.5 \cdot \text{Dose}_0 + \\ &\quad 4 \cdot \sqrt{\text{Weight}} - 10 \cdot \text{Age}) \\ \text{logit}^{-1}(-8 + 0.5 \cdot \text{Dose}_0 + \\ &\quad 8.568 \cdot \sqrt{\text{Weight}} - 9.060 \cdot \text{Age}) \\ \text{logit}^{-1}(20 + 0.5 \cdot \text{Dose}_0 + \\ &\quad 6.562 \cdot \sqrt{\text{Weight}} - 18.325 \cdot \text{Age}) \end{cases} \\
\text{EFV} &\sim \mathcal{N}_{\text{trunc}}(\mu = 0.1 \cdot \text{Dose} + 0.1 \cdot \text{MEMS} + 2.66 \cdot \mathbb{1}_{\{\text{Genotype} \leq 2\}} \\
&\quad + 4.6 \cdot \mathbb{1}_{\{\text{Genotype} = 3\}}, \sigma = 4.06, l = 0.2032, h = 21.84, \\
&\quad l_a = 0.2032, l_b = 0.88, h_a = 8.37, h_b = 21.84) \\
\text{VL} &\sim \text{Bernoulli}(p = 1 - \text{logit}^{-1}(0.4 + 0.1 \cdot \text{CoMo} \\
&\quad + 2 \cdot \sqrt{\text{EFV}}))
\end{aligned}$$

The distribution $\mathcal{N}_{\text{trunc}}(\mu, \sigma, l, h, l_a, l_b, h_a, h_b)$ represents a truncated normal distribution, where l and h are the truncation thresholds. Values less than l are replaced with random draws from a $U(l_a, l_b)$ distribution, while values greater than h are replaced with random draws from a $U(h_a, h_b)$ distribution. Here, U denotes a continuous uniform distribution.

C Estimate the Conditional Density via Hazard Binning

Consider discretizing the observed variable a into T bins using an appropriate binning procedure. Given this, we can estimate the probability of a falling into the interval $[\alpha_{t-1}, \alpha_t]$, $t = 1, \dots, T$, using a standard classification model. Within each bin $[\alpha_{t-1}, \alpha_t]$, the density is assumed to undergo a uniform transformation, leading to the following expressions:

$$\begin{aligned}
P(a \in [\alpha_{t-1}, \alpha_t] | \mathbf{L}) &= P(a \in [\alpha_{t-1}, \alpha_t] | A \geq \alpha_{t-1}, \mathbf{L}) \times \\
&\quad \prod_{j=1}^{t-1} \{1 - P(a \in [\alpha_{t-1}, \alpha_t] | A \geq \alpha_{j-1}, \mathbf{L})\} \\
f(a | \mathbf{l}) &= \frac{P(a \in [\alpha_{t-1}, \alpha_t] | \mathbf{L})}{\alpha_t - \alpha_{t-1}}
\end{aligned}$$

To obtain the density, we can apply either parametric or non-parametric estimation to the hazard model and then transform the results into a density for each bin. This approach is adapted from Haldensify, proposed by Nima S. Hejazi et al. [15, 14, 16], and it is similar to the approach described in an earlier proposal [10].

D Simulation 1: Bootstrap CI coverage probabilities

See Figure 8.

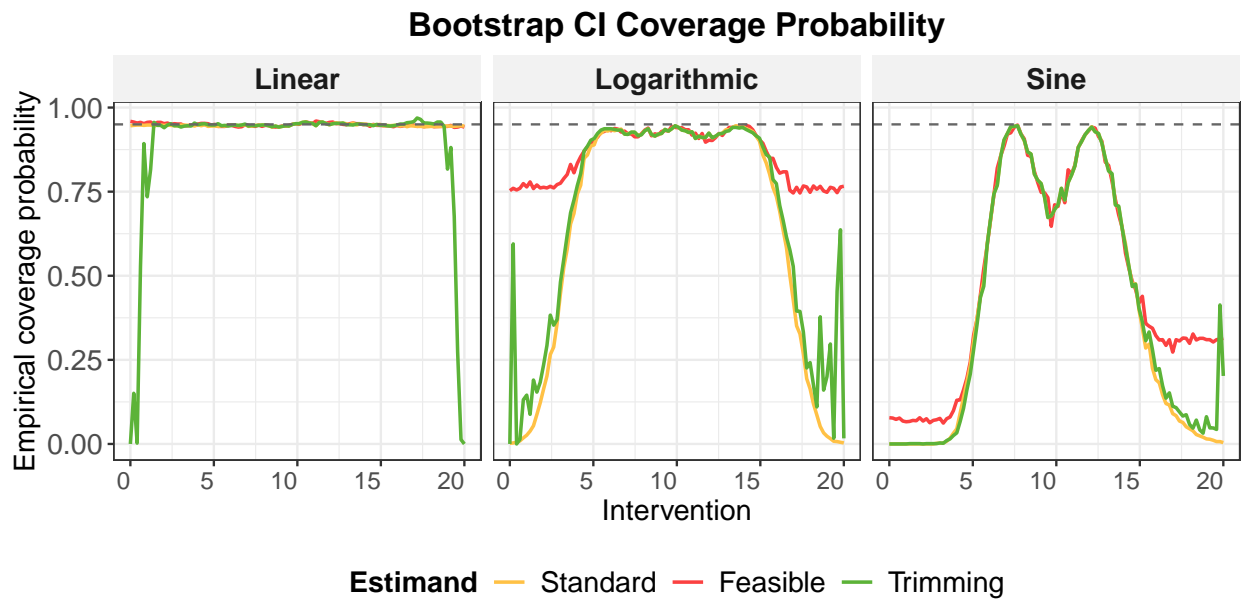


Figure 8: **Bootstrap CI coverage probabilities in Simulation 1.** Empirical coverage of 95% bootstrap confidence intervals for three estimators—Standard (orange), Feasible (red), and Trimming (green)—as a function of the intervention value A . Each panel corresponds to a different true outcome function: Linear, Logarithmic, or Sine. The horizontal dashed line indicates the nominal 95% coverage level. When the outcome is linear (correctly specified by the model), all estimators achieve near-nominal coverage. Under nonlinear outcomes (model misspecification), the Standard estimator shows undercoverage in regions with limited support, while the Trimming estimator attains nominal coverage in well-supported areas but becomes unstable near the boundaries. The Feasible estimator provides stable coverage across the intervention range, achieving nominal levels when the outcome model is correctly specified, and offering more reliable coverage under misspecification.